JVI Journals.ASM.org

Oxylipin Biosynthesis Genes Positively Regulate Programmed Cell Death during Compatible Infections with the Synergistic Pair *Potato Virus X-Potato Virus Y* and *Tomato Spotted Wilt Virus*

Alberto García-Marcos, Remedios Pacheco, Aranzazu Manzano, Emmanuel Aguilar, Francisco Tenllado

Departamento de Biología Medioambiental, Centro de Investigaciones Biológicas, CSIC, Madrid, Spain

One of the most severe symptoms caused by compatible plant-virus interactions is systemic necrosis, which shares common attributes with the hypersensitive response to incompatible pathogens. Although several studies have identified viral symptom determinants responsible for systemic necrosis, mechanistic models of how they contribute to necrosis in infected plants remain scarce. Here, we examined the involvement of different branches of the oxylipin biosynthesis pathway in the systemic necrosis response caused either by the synergistic interaction of *Potato virus X* with *Potato virus Y* (PVX-PVY) or by *Tomato spotted wilt virus* (TSWV) in *Nicotiana benthamiana*. Silencing either *9-lipoxygenase* (*LOX*), *13-LOX*, or α-*dioxygenase-1* (α-*DOX-1*) attenuated the programmed cell death (PCD)-associated symptoms caused by infection with either PVX-PVY or TSWV. In contrast, silencing of the jasmonic acid perception gene, *COI1* (Coronatine insensitive 1), expedited cell death during infection with compatible viruses. This correlated with an enhanced expression of oxylipin biosynthesis genes and dioxygenase activity in PVX-PVY-infected plants. Moreover, the *Arabidopsis thaliana* double *lox1* α-*dox-1* mutant became less susceptible to TSWV infection. We conclude that oxylipin metabolism is a critical component that positively regulates the process of PCD during compatible plant-virus interactions but does not play a role in restraining virus accumulation *in planta*.

Plant viruses are responsible for severe diseases in plants, resulting in major losses in many important crops. The development of symptoms is likely to be the result of a complex interplay between plant and virus in the context of cellular homeostasis. Some symptoms of viral infections are the result of alterations in plant growth and development. In particular, connections between the interactions of specific virus factors and cell components that cause alterations in hormone synthesis and signaling have been noted (reviewed in references 1 and 2). Recent studies of gene expression profiles in various pathosystems have shown that sets of defense-related genes are expressed upon the infection of susceptible plants with several different viruses (3, 4), suggesting that even susceptible plants recognize virus infection and mount defense responses. The discovery of coordinated induction of defense-related genes in compatible plant-virus interactions has led to investigation of the effects of their induced expression on virus accumulation and symptomatology (5, 6, 7). These alterations in defense gene expression might not necessarily provide a line of defense against virus infection but may have adverse effects on host metabolism that contribute to disease symptom development.

One of the most severe symptoms elicited by plant viruses is systemic necrosis, which can lead to the death of the plant over the course of several days. In several compatible pathosystems, close relationships between defense responses to virus infection and severe necrotic symptoms have been reported (8, 9, 10). Several studies have postulated that systemic necrosis shares hypersensitive response (HR) attributes as a consequence of delayed occurrence of biochemical and physiological events that are associated with programmed cell death (PCD) (10, 11). We have shown that coinfection of *Nicotiana benthamiana* with *Potato virus X* and *Potato virus Y* (PVX-PVY) resulted in systemic necrosis (synergism in pathology), which correlated with the transcriptional activation of defense-related genes (9). Further detailed analysis of transcriptomic data identified the oxylipin biosynthesis pathway as a category of genes uniquely upregulated by PVX-PVY but not by single infection with PVX or PVY.

Oxylipins are a large family of lipid-derived metabolites that regulate many defense and developmental pathways in plants (12). These compounds are produced by initial dioxygenation of polyunsaturated fatty acids, mainly linolenic and linoleic acids, by the action of lipoxygenases (9-LOX and 13-LOX), α-dioxygenases (α-DOX), and monoxygenases, followed by secondary modifications catalyzed by other enzymatic activities (13). The production of oxylipins from polyunsaturated fatty acids can also take place nonenzymatically in the presence of singlet oxygen or by free radical-mediated oxygenation (14).

Our understanding of functional aspects of oxylipin pathways comes mainly from the studies of jasmonic acid (JA) and their derivatives, methyl jasmonate (MeJA) and Ile-JA. These molecules are derived from the action of 13-LOX on linolenic acid and serve key signaling roles in the transduction pathways that regulate the expression of certain defense-related and developmental genes (15, 16). Coronatine insensitive 1 (COI1) is an F-box protein and has been implicated in jasmonate-regulated defense responses (17). COI1 serves as a receptor for an Ile-conjugated form of JA and activates the JA signaling pathway.

Besides 13-LOX-generated oxylipins, several studies demonstrated the participation of the α-DOX-1 and 9-LOX pathways in the regulation of several aspects of plant development and defense

Received 4 January 2013 **Accepted** 4 March 2013
Published ahead of print 13 March 2013
Address correspondence to Francisco Tenllado, tenllado@cib.csic.es.

doi:10.1128/JVI.03573-12

through a JA-independent signaling pathway (18, 19). Thus, genetic studies revealed the role of α-DOX-1 and 9-LOX in the defense response of tobacco and *Arabidopsis* to fungal and bacterial attack, likely by regulating oxidative stress and cell death (20, 21, 22, 23). Interestingly, several oxylipins that originate from 9- and 13-LOX activities were found to be sufficient to initiate PCD and HR in different pathosystems (24, 25, 26). In addition, JA has been implicated in the signaling cascade leading to LOX elicitation. Methyl jasmonate (MeJA) treatment was reported to induce LOX activities and the transcription of the corresponding genes in plants (24, 27). Little information is available about the role of oxylipins in virus-infected plants. Several lines of evidence suggest that oxylipins play an important role in the development of HR and disease resistance (28, 29). Moreover, the application of MeJA on plants was effective in inhibiting the replication of several viruses, including PVY, in compatible pathosystems (30, 31, 32).

In previous studies, virus-induced gene silencing (VIGS) of α-*DOX-1* in *N. benthamiana* delayed cell death during PVX-PVY infection (9). Since α-*DOX-1* competes with other branches of oxylipin metabolism for common substrate fatty acids (21) and because of the complex cross talk between oxylipins and other phytohormones in plant-pathogen interactions (23), unequivocal evidence for the involvement of oxylipins in virus pathogenicity is still lacking. In this study, we tested the involvement of different branches of the oxylipin biosynthesis pathway in the systemic necrosis response during compatible viral infections in *N. benthamiana* and further characterized the involvement of α-DOX-1 and 9-LOX pathways in virus pathogenicity in *Arabidopsis thaliana*. We demonstrated that oxylipin-mediated cell death during compatible plant-virus interactions did not restrain virus accumulation *in planta*, since a delay in oxylipin-mediated cell death did not result in increased accumulation of virus. Furthermore, we showed that silencing of *COI1* expedited cell death in *N. benthamiana* during compatible plant-virus interactions, which correlated with an enhanced expression of oxylipin biosynthesis genes and dioxygenase activity. Therefore, we conclude that oxylipin metabolism is a critical component that positively regulates the process of PCD during compatible plant-virus interactions.

MATERIALS AND METHODS

Plant material and inoculations. *N. benthamiana* plants were grown in a growth chamber with a 16-h-light/8-h-dark cycle at 25°C. Four-week-old *N. benthamiana* plants were inoculated by rubbing plant sap infected with PVX, PVY, or *Tomato spotted wilt virus* (TSWV) onto two fully expanded leaves as described previously (33). Mixed inoculations were performed separately on opposite halves of the same leaves. Control plants were mock inoculated with extracts from healthy leaves, and the leaves were harvested at the same time points as those of the infected plants.

The homozygous *A. thaliana* double insertion mutant *lox1* α-*dox-1* has been previously characterized by Vicente et al. (23). Seeds were sown on soil, vernalized for 3 days at 4°C, and grown in a chamber at 22°C under a 14-h-light/10-h-dark photoperiod. Plants were inoculated 4 weeks after germination with plant sap infected with TSWV. The transgenic *N. benthamiana* plants expressing the salicylate hydroxylase gene have been described previously (34).

Detection of defense-associated responses. For cell death analyses, leaf discs detached from upper leaves were stained with lactophenol-trypan blue as described previously (21). For 3,3′-diaminobenzidine (DAB) staining to detect H_2O_2 production, leaves were vacuum infiltrated for 2 min with DAB solution at 1 mg/ml (35). Superoxide (O_2^-) generation was detected using nitroblue tetrazolium (NBT) staining as described previously (36). Leaves for autofluorescence experiments were prepared as described previously (37). The terminal deoxynucleotidyltransferase-mediated dUTP nick end labeling (TUNEL) assay was performed using the *in situ* cell death detection kit with fluorescein (Roche Diagnostics), as described by Pacheco et al. (38). Consecutive slides were treated with 4′,6-diamidino-2-phenylindole (DAPI) for nuclear staining. Representative phenotypes were photographed with a Leica L2 stereoscope and Leica DM 2500 microscope using a Leica DFC 320 camera.

Measurement of electrolyte leakage. Cell damage was assayed by measuring electrolyte leakage. Twenty-five disks of 0.3 cm^2 were excised from upper leaf tissue using a core borer. Disks were rinsed briefly with water and floated on 5 ml of double distilled water for 6 h at room temperature. The conductivity of the water was measured using a Crison conductivity meter. This represented the electrolyte leakage from the leaf discs (reading 1). Then, samples were boiled for 20 min at 90°C. After the liquid cooled down, the conductivity of the water was measured again. This represented the total ions present in the leaf discs (reading 2). Electrolyte leakage was represented as the percentage of total ions released [(reading 1/reading 2) × 100]. Reported data are means and standard errors of the values obtained in three independent experiments with pools from 5 to 10 plants for each treatment. Statistical analyses (analysis of variance [ANOVA] followed by Duncan's multiple range test) were performed using the statistical software Statgraphics plus 5.1 (Statistical Graphics Corp).

Real-time quantitative RT-PCR and RT-PCR analyses. Total RNA was extracted from upper, noninoculated leaves at different times postinoculation using TRIzol reagent (Invitrogen), followed by purification with RNeasy midiprep columns (Qiagen). Real-time quantitative reverse transcription (RT)-PCR (qRT-PCR) reactions were performed in the Rotor-Gene 6000 real-time PCR detection system (Corbett). One-step qRT-PCR was performed using total RNA preparations treated with a Turbo DNA-free kit (Ambion). The real-time assay was performed using 15 μl of a reaction mixture that contained 7.5 μl of brilliant III ultrafast qRT-PCR master mix (Agilent), 1.8 μl of RNase-free water, 0.75 μl of reverse transcriptase, 0.15 μl 100 mM dithiothreitol (DTT), 0.3 μM each primer (available upon request), and 3 μl of total RNA extract (~10 ng RNA/μl). qRT-PCRs with and without reverse transcriptase were run in parallel, to ensure the absence of DNA template in the samples. qRT-PCR was carried out at 50°C for 10 min, 95°C for 3 min, 40 cycles of 95°C for 10 s, and 60°C for 20 s. All reactions were done in triplicate with two replicates of each sample in each run. Three independent biological replicates for each treatment were used for qRT-PCR analyses, and the values obtained averaged. The amplification efficiency was determined for each primer pair with a 5-fold serial dilution of an RNA sample (~100 ng RNA/μl) with at least five dilution points. Synthesis of cDNA products of about 150 bp in length was confirmed by melting curve analysis using the Rotor-Gene 6000 software. The relative quantification of PCR products was calculated by the comparative ΔΔ*CT* (cycle threshold) method. 18S rRNA was chosen for normalization because of its similar level of expression across all treatments. To clarify the graphics used to report the results of each experiment, the value of a control sample was set at 1 and other data calculated relative to this value.

For RT-PCR analyses, first-strand cDNA was synthesized using 0.64 μg of total RNA, 0.5 μM oligo(dT) primer (Invitrogen), and SuperScript II reverse transcriptase (Invitrogen) to a final volume of 20 μl. PCR was performed in 20-μl reaction mixtures using 4 μl cDNA, 1× PCR buffer, 200 μM deoxynucleoside triphosphate (dNTP), 0.5 μM each gene-specific primer (available upon request), and 0.2 units of Phusion high-fidelity DNA polymerase (Finnzymes). To ensure that similar amounts of cDNA were used for silenced and nonsilenced plants, amplification of *RPL3A* or actin was used as the internal control for *Arabidopsis* or *N. benthamiana*, respectively. Each PCR cycle included denaturation at 98°C for 15 s, annealing at 60°C for 30 s, and elongation at 72°C for 20 s. Aliquots were removed from the thermocycler after 25, 30, and 35 cycles for virus detection and after 30, 33, and 36 cycles for mRNA detection. These cycles of amplification were within the log-linear phase of PCR

product amplification in the nonsilenced control sample. A PCR using template derived from RNA without reverse transcription was performed as a negative control. The aliquots were analyzed on a 1.5% agarose gel stained with ethidium bromide. The RT-PCR analysis was repeated for two independent groups of silenced plants with similar results.

VIGS assays. A 703-bp fragment of *N. benthamiana 9-LOX* (*Nb9-LOX*), a 580-bp fragment of *Nb13-LOX*, a 466-bp fragment of *Nb*α*-DOX-1*, and a 174-bp fragment of *NbCOI1* were amplified and introduced into the binary vector pTRV2 to generate pTRV2:*9-LOX*, pTRV2:*13-LOX*, pTRV2:*DOX-1*, and pTRV2:*COI1*, respectively (39). The primer pairs used to amplify these genes are available upon request. The pTRV1 vector and the pTRV2 vector and its derivatives were separately transformed into *Agrobacterium tumefaciens* strain GV2260. *N. benthamiana* leaves were infiltrated with *A. tumefaciens* cultures as described previously (40).

Total RNA was extracted from upper, noninoculated leaf tissue at 10 days after infiltration. Silencing of mRNAs was detected by qRT-PCR as described above. Primers that anneal outside the region targeted for silencing were used to ensure that the endogenous gene is tested.

Plant transformation for RNA interference (RNAi)-mediated silencing. Transgenic silencing of *COI1* in *N. benthamiana* plants was carried out by means of a 174-bp fragment that encompasses nucleotides 1292 to 1465. This fragment was PCR amplified from the pTRV2:*COI1* clone using primer sequences 5′GCCACTTGATAATGGTGT and 5′AG AGGCCTTCATCGGAT, bearing at their 5′ ends the attB1 and attB2 recombinant sequences, respectively. The PCR product was cloned into the donor plasmid pDONR207 by BP clonase II recombination (Gateway technology; Invitrogen). The *COI1* fragment from pDONR207 was transferred into the binary destination vector pH7GWIWG2(II) (41) using LR clonase II (Invitrogen). pH7GWIWG2(II) contains a chloramphenicol resistance marker (Cm^R) and two *ccdB* genes flanked by recombinant attR1 and attR2 sequences in inverse orientations, separated by an intron. Recombination replaced the *ccdB* genes with the *COI1* fragment, yielding a hairpin construct able to trigger *COI1* mRNA degradation. Restriction enzyme digestion was used to verify the recombinant construct.

N. benthamiana leaf disks were infected with *A. tumefaciens* GV2260 transformed with the RNAi recombinant plasmid in accordance with the methods of Ying et al. (34). Hygromycin-resistant plants were regenerated, and T2 progeny were analyzed for *NbCOI1* expression and MeJA responsiveness.

Protein extraction and dioxygenase assays. Plant tissues were ground in liquid nitrogen and homogenized in 100 mM sodium phosphate buffer (pH 6.5) in the proportion of 1 ml extraction buffer per 0.5 g of tissue. The homogenate was centrifuged at 15,000 × *g* for 30 min at 4°C. The protein content of the crude extract was determined by the method of Bradford (42). Dioxygenase activity in the soluble fractions was spectrophotometrically measured by monitoring the increase of the conjugated diene hydroperoxide at A_{234} at 25°C for 10 min (43). The assay mixture included 100 mM sodium phosphate buffer (pH 6.5), 0.1 mM linoleic acid (Sigma), and 5 to 10 μl of resuspended enzyme in a total volume of 1.0 ml. The reaction was also performed in the presence of 1 mM KCN to verify that the enzymatic activity was cyanide resistant. Dioxygenase specific activity was expressed in nkat mg^{-1} protein using a molar extinction coefficient of 25,000 M^{-1} cm^{-1}.

Hormone treatments. Four-week-old *N. benthamiana* plants were sprayed with MeJA (250 μM), salicylic acid (SA) (2 mM), abscisic acid (ABA) (100 μM), 1-aminocyclopropane-1-carboxylic acid (ACC) (2 mM) (Sigma) or water every day from 1 day before the inoculation to 5 days postinoculation (d.p.i.). Four-week-old *A. thaliana* plants were sprayed with MeJA (100 μM) from 1 day before the inoculation to 16 d.p.i. The treated plants were sampled at various time points after inoculation to determine electrolyte leakage and virus accumulation.

Sequence data. Sequence data used for this article can be found in the EMBL/GenBank data libraries under accession numbers X84040 (*9-LOX*), AY254349 (*13-LOX*), AJ007630 (α*-DOX-1*), EF025087 (*COI1*), D90196 (*PR-1*), AF229927 (*TD*), DQ158182 (*PI-I*), AJ236016 (18S rRNA), AY179605 (*ACT*), At1g43170 (*RPL3A*), M95516 (PVX), Z50043 (PVY), and NC_002052 (TSWV).

RESULTS

Systemic necrosis induced by PVX-PVY is associated with defense responses. To examine whether plants doubly infected with PVX and PVY express defense-associated responses, several histochemical, biochemical, and molecular markers usually associated with cell death were analyzed in upper, noninoculated leaves. Trypan blue was used to selectively stain dead cells. At 8 d.p.i., blue staining was observed in PVX-PVY-infected leaves but not in leaves of plants infected with either PVX or PVY alone (Fig. 1A and data not shown). A characteristic brown color was detected in PVX-PVY-infected leaves stained with DAB, indicating H_2O_2 production (Fig. 1B). Superoxide (O_2^-) production in leaves of doubly infected plants was also determined by staining with NBT. We then monitored electrolyte leakage as a quantitative indicator of the extent of cell membrane injury. Consistent with the above-described results, plants infected with PVX-PVY exhibited significantly greater electrolyte leakage levels than control plants and plants infected with either PVX or PVY (Fig. 1C). Cell death lesions in plants can be visualized by fluorescence under UV light, indicating the cell death-related production of phenylpropanoid metabolites (44). UV illumination revealed the accumulation of autofluorescent compounds in regions corresponding to areas of necrosis (veins) in PVX-PVY-infected leaves. Plants infected with either PVX or PVY did not show autofluorescence (Fig. 1D).

Degradation of nuclear DNA is one of the hallmarks of PCD. We have therefore utilized an assay based on the detection of 3′ hydroxyl groups of degraded nuclear DNA (TUNEL assay) (45) to investigate whether PCD was involved in the systemic necrosis induced by PVX-PVY. Green fluorescence indicated that DNA fragmentation had occurred in the sections from PVX-PVY-infected leaves but not in sections from PVX- or PVY-infected leaves (Fig. 1E). Together, these results suggest that systemic necrosis induced by the synergistic interaction of PVX with PVY in *N. benthamiana* is associated with PCD.

Attenuated virulence of PVX-PVY in plants silenced for oxylipin biosynthesis genes. Microarray data from early studies indicated that the oxylipin biosynthesis pathway is induced after infection with PVX-PVY (9). Here, qRT-PCR analyses showed that *N. benthamiana* homologues of *Nicotiana tabacum LOX1* (9-LOX activity) (46), *Nicotiana attenuata LOX3* (13-LOX activity) (47), and *N. tabacum* α*-DOX-1* (48) were, indeed, induced at higher levels in PVX-PVY-infected plants than in plants infected with either PVX or PVY at early stages of the infection process (6 d.p.i.) (Fig. 1F), before cell death was observed by trypan blue staining (data not shown).

To evaluate the function of oxylipin biosynthesis genes in the systemic necrosis induced by PVX-PVY, VIGS analysis was conducted in *N. benthamiana* for genes that initiate each of the three main biosynthetic branches leading to oxylipins, i.e., *9-LOX*, *13-LOX*, and α*-DOX-1*. Fragments of *N. benthamiana* homologues of the genes used for qRT-PCR measurements were cloned separately into a *Tobacco rattle virus* (TRV)-based VIGS vector. *N. benthamiana* plants were infiltrated with a recombinant vector or the empty vector (TRV2:00) as a control. At 10 days after infiltration (d.a.i.), plants were either mock inoculated or challenge inoculated with PVX-PVY in upper, noninfiltrated leaves. Gene silencing efficiency was examined by qRT-PCR in the mock-inoc-

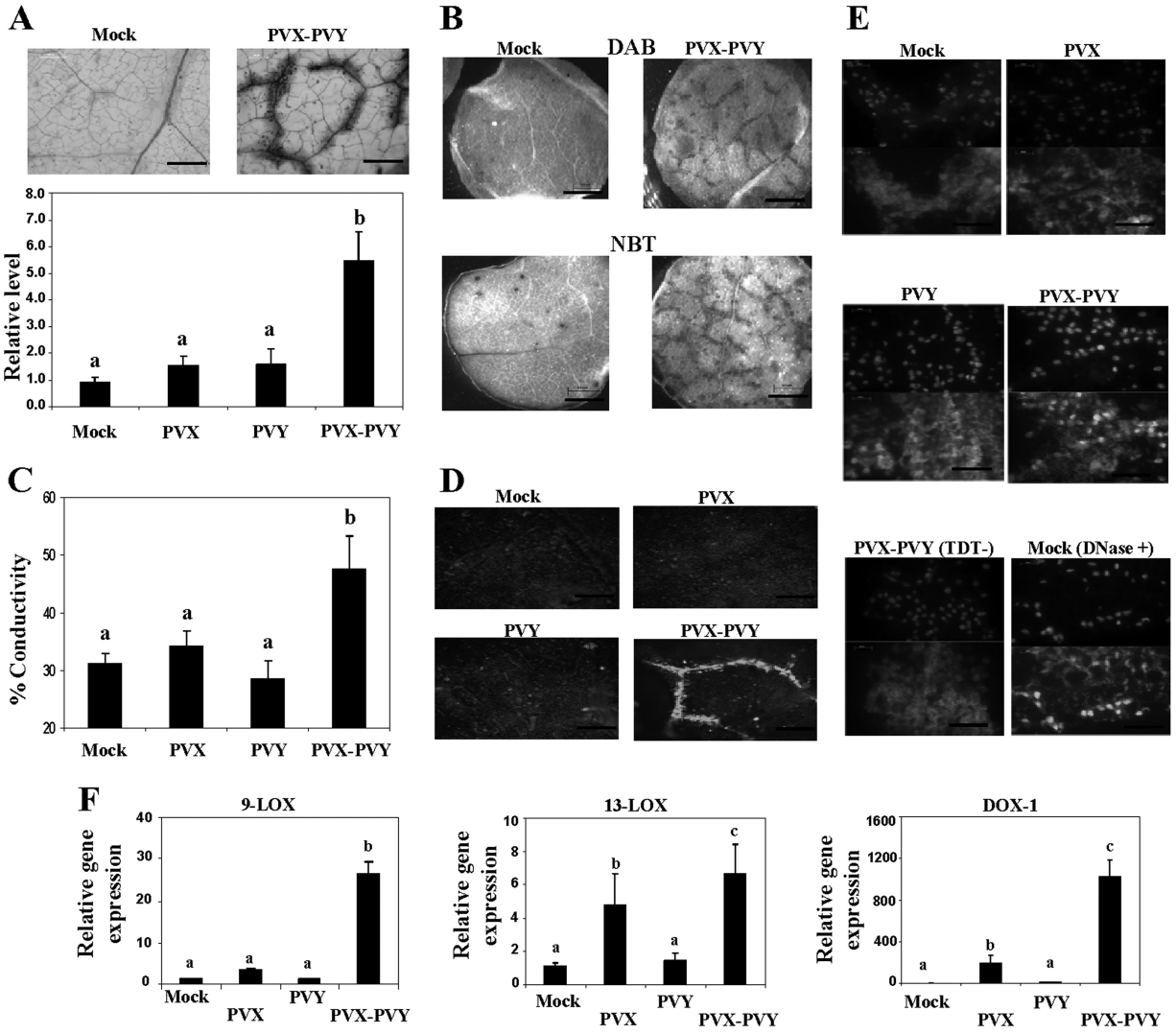

FIG 1 Dead cells and reactive oxygen species in upper leaves of *N. benthamiana* plants doubly inoculated with PVX and PVY. (A) Leaf discs from plants inoculated with PVX, PVY, or PVX-PVY and from mock-inoculated plants were stained with trypan blue for 1 min and then decolorized in chloral hydrate solution overnight. (Top) Cell death sites could be visualized as a dark coloration in the PVX-PVY sample at 8 days postinoculation (d.p.i.). Scale bars = 0.2 mm. (Bottom) The absorbance of the dye was measured spectrophotometrically at 590 nm using a microtiter plate reader. (B) Leaf discs from plants inoculated with PVX-PVY and mock-inoculated plants were stained with either DAB or NBT solution at 8 d.p.i. O_2^- production was visualized as a dark blue coloration. DAB formed a deep-brown polymerization product upon reaction with H_2O_2. Scale bars = 1 mm. (C) Electrolyte leakage from leaf discs of virus-infected plants and mock-inoculated plants at 8 d.p.i. (D) Accumulation of defense-related phenylpropanoid metabolites (gray) was visualized by UV illumination at 8 d.p.i. Scale bars = 0.2 mm. (E) Detection of nuclear DNA fragmentation in plants infected with PVX-PVY. Transferase-mediated dUTP nick-end labeling (TUNEL) assay (lower panels) was performed in leaf sections from PVX-, PVY-, PVX-PVY-, and mock-inoculated plants at 8 d.p.i. Sections of a PVX-PVY-inoculated plant were not treated with the terminal deoxynucleotidyl transferase enzyme (TDT−) as a negative control. Sections of a mock-inoculated plant were treated with DNase I (DNase +) as a positive control. Nuclei are indicated by 4′,6-diamidino-2-phenylindole (DAPI) staining (upper panels). Scale bars = 50 μm. (F) qRT-PCR analysis of expression of the *9-LOX*, *13-LOX*, and α-*DOX-1* genes in *N. benthamiana* leaves 6 days after inoculation with PVX and PVY. Expression of the 18S rRNA gene served as a control. Data represent the means ± standard errors of three replicates, each consisting of three to five plants that received the same treatment. Statistically significant differences between means were determined by employing Duncan's multiple range test. Different letters indicate significant differences at a *P* value of 0.05.

ulated plants (Fig. 2). Transcripts of the target genes *9-LOX*, *13-LOX*, and α-*DOX-1* accumulated to much lower levels in the VIGS-treated plants than in the control plants. The expression of *9-LOX* and *13-LOX* was also reduced, albeit less significantly, by heterologous sequences. Given that *9-LOX*, *13-LOX*, and α-*DOX-1* do not share significant stretches of nucleotide identity with each other, these second-level changes could probably be the result of cross talk between metabolic pathways in the complex networks of oxylipin production. In this sense, oxylipin biosynthesis genes compete for common substrate fatty acids and can also operate on oxygenated fatty acids, resulting in, for instance, *9-LOX*-α-*DOX-1* doubly oxygenated products (19).

Systemic mosaic symptoms developed simultaneously in both VIGS-treated and control (TRV2:00) plants at 6 d.p.i. with PVX-PVY. Eight days after inoculation, the control plants started to show the necrosis symptoms typical of the viral synergistic inter-

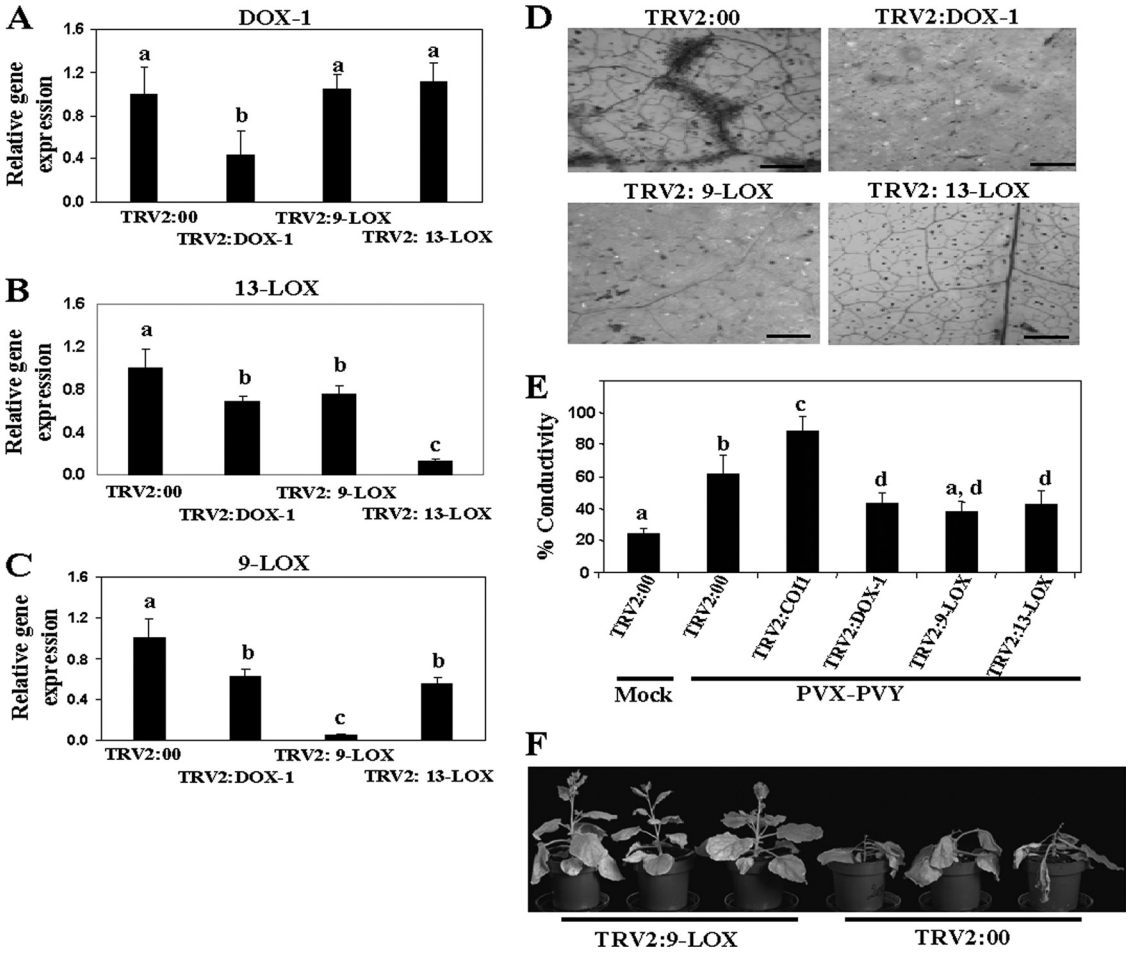

FIG 2 Silencing of *N. benthamiana 9-LOX*, *13-LOX*, and α-*DOX-1* result in attenuated cell death induced by PVX-PVY infection. (A to C) Three-week-old *N. benthamiana* plants were infiltrated with *Agrobacterium* containing TRV2:*DOX-1*, TRV2:*9-LOX*, TRV2:*13-LOX*, or TRV2:00 (vector control). The relative levels of expression of α-*DOX-1* (A), *13-LOX* (B), and *9-LOX* (C) were estimated by qRT-PCR 10 days after infiltration (d.a.i.). Expression of the 18S rRNA gene served as a control. (D) Plants agroinfiltrated with TRV2:*DOX-1*, TRV2:*9-LOX*, TRV2:*13-LOX*, TRV2:*COI1*, or TRV2:00 (vector control) were inoculated with PVX-PVY at 10 d.a.i. Uppermost leaves of control and VIGS-treated plants were stained with trypan blue to detect cell death at 8 days postinoculation (d.p.i.). Scale bars = 0.1 mm. (E) Leaf discs were excised and assayed for electrolyte leakage at 8 d.p.i. Data represent the means ± standard errors of five replicates, each consisting of three to five plants that received the same treatment. Statistically significant differences between means were determined by employing Duncan's multiple range test. Different letters indicate significant differences at a *P* value of 0.05. (F) Effect of *9-LOX* silencing on PVX-PVY infection at 12 d.p.i. Control plants exhibited the typical necrosis symptoms associated with the synergistic viral interaction, while *9-LOX*-silenced plants exhibited mosaic symptoms but not systemic necrosis.

action. In contrast, *9-LOX*-, *13-LOX*-, and α-*DOX-1*-silenced plants exhibited only mosaic symptoms with no visible necrosis at this time point. Consistent with these observations, trypan blue staining (Fig. 2D) and electrolyte leakage measurement (Fig. 2E) revealed dramatically reduced cell death in *9-LOX*-, *13-LOX*-, and α-*DOX-1*-silenced leaves compared with that in nonsilenced control leaves. Mock-inoculated silenced plants exhibited levels of electrolyte leakage similar to the levels in control plants (data not shown). Eventually, silenced plants showed signs of necrosis at late stages of the infection process with differences in its extent, with the *9-LOX*-silenced plants being less affected by the virus infection (Fig. 2F). Comparative analysis of virus accumulation by RT-PCR revealed that the levels of PVX RNA and PVY RNA at 8 d.p.i. in *9-LOX*-, *13-LOX*-, and α-*DOX-1*-silenced plants were similar to the levels in control plants, ruling out the possibility that the delayed cell death was due to limited virus spread or accumulation in silenced plants (Fig. 3). These data prompted the hypothesis that oxylipin biosynthesis genes act as virulence factors in the compatible interaction of PVX-PVY with *N. benthamiana*.

Enhanced virulence of PVX-PVY in *COI1*-silenced plants. We speculated whether the attenuated virulence of PVX-PVY in plants silenced for oxylipin biosynthesis genes is due to alteration in JA signaling. Although JA is exclusively produced through the 13-LOX pathway, targeting *LOX-9* and α-*DOX-1* by VIGS partially affected *13-LOX* expression (Fig. 2). To assess a functional role of JA signaling in the systemic necrosis induced by PVX-PVY, we silenced *COI1* by VIGS. *COI1* participates in JA perception and regulates gene expression by promoting degradation of transcriptional repressors (17). In contrast to the induction of oxylipin biosynthesis genes by PVX-PVY infection, *COI1* expression was repressed in doubly infected plants (Fig. 4A). *N. benthamiana* plants were infiltrated with a recombinant vector carrying a fragment of *NbCOI1* (TRV2:*COI1*) or TRV2:00 as a control. At 10 d.a.i., the transcript level of *COI1* was significantly reduced in the

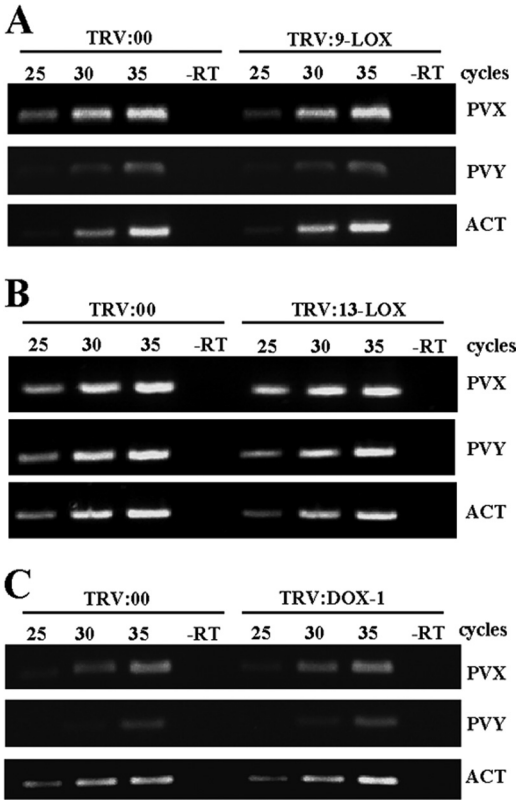

FIG 3 Comparison of relative viral loads estimated by RT-PCR in control plants and plants with silenced *9-LOX* (A), *13-LOX* (B), and α-*DOX-1* (C) at 8 days after inoculation with PVX-PVY. The same RT reactions were used to amplify actin gene transcripts as a control. The numbers of PCR cycles are indicated for each treatment. −RT, control without RT.

silenced plants compared to its level in control plants (Fig. 4B). No significant differences in the expression of *9-LOX* and *13-LOX* mRNAs were found between *COI1*-silenced and control plants, although a slight increase of α-*DOX-1* expression was detected in *COI1*-silenced plants (Fig. 4C). Otherwise, silencing of *9-LOX*-, *13-LOX*-, and α-*DOX-1* had negligible effects on *COI1* mRNA expression.

Then, we examined the response of *COI1*-silenced plants to PVX-PVY infection. The cell death-associated disease symptoms were observed about 2 days earlier in the *COI1*-silenced plants (6 d.p.i.) than in the control plants. Silencing of *COI1* caused slightly retarded plant growth, although mock-inoculated *COI1*-silenced plants remained free of necrotic symptoms throughout the trial period. To characterize the observed necrotizing process at the microscopic level, cell death and O_2^- production were detected by staining with trypan blue and NBT, respectively (Fig. 4D and E). The development of the necrosis response and reactive oxygen species (ROS) production was faster and stronger in *COI1*-silenced plants than in control plants. Consistent with these observations, *COI1*-silenced plants infected with PVX-PVY exhibited significantly higher levels of electrolyte leakage than control plants (Fig. 2E). Typical disease symptoms with no sign of necrosis developed in *COI1*-silenced plants singly infected with either PVX or PVY (data not shown). To examine whether the enhanced cell death phenotype was associated with changes in the accumulation of PVX and/or PVY, we monitored the amounts of viruses in infected leaves from *COI1*-silenced and control plants by RT-PCR (Fig. 4F). The accumulation of PVX and PVY did not show differences between the *COI1*-silenced plants and the controls. The above-described results were further confirmed by measuring viral RNA accumulation using qRT-PCR (Fig. 4G). These data indicate that reduced expression of *COI1* in *N. benthamiana* accelerates cell death during infection with PVX-PVY but does not affect viral accumulation.

We further evaluated whether *COI1* silencing affects the expression of oxylipin biosynthesis genes in response to PVX-PVY infection. The expression levels of oxylipin genes in *COI1*-silenced and nonsilenced control plants were analyzed at 6 d.p.i. by RT-PCR. As shown by the results in Figure 5A, PVX-PVY infection remarkably induced higher levels of *9-LOX*-, *13-LOX*-, and α-*DOX-1* mRNAs in *COI1*-silenced plants than in control plants. In contrast, the expression of *COI1* in *9-LOX*-silenced plants was similar to that in control plants (Fig. 5B). The effect of silencing oxylipin biosynthesis and perception genes in salicylic acid (SA) signaling was also determined by comparing *PR-1* gene expression in control and VIGS-treated plants. No significant difference in *PR-1* mRNA levels was found between *COI1*- and *9-LOX*-silenced plants and control plants (Fig. 5C). Collectively, these results suggest a negative cross talk between the oxylipin biosynthesis pathways and *COI1*-mediated signaling during PVX-PVY infection.

Enhanced dioxygenase activity in *NbCOI1* IR transgenic plants. One drawback to VIGS is that sometimes it may not produce uniform silencing throughout the plant, which could complicate the interpretation of results. We therefore generated transformants of *N. benthamiana* in which *COI1* was silenced by an RNAi hairpin construct. The *NbCOI1* inverted repeat (IR) lines showed slightly retarded growth, with occasional rolling of the leaf blades into a cup-shaped form. Most *NbCOI1* IR lines yielded low seed production, which is in accord with a role of *COI1* of *N. attenuata* in its fertility (49). Therefore, T2 seeds from a less-affected *NbCOI1* IR line (line 7) were pooled for functional analysis. RT-PCR analysis showed that *NbCOI1* expression was significantly downregulated in *NbCOI1* IR plants (Fig. 6A). Expression of the JA-dependent response gene *threonine deaminase* (*TD*), which is involved in converting Thr to Ile for JA-Ile biosynthesis (50), was induced by MeJA in wild-type (WT) plants but not in *NbCOI1* IR plants, suggesting that JA responsiveness is altered in *NbCOI1* IR plants (Fig. 6B). Upon PVX-PVY infection, necrosis developed 2 days earlier in *NbCOI1* IR plants than in WT plants (Fig. 6D). As described above for plants that were *COI1* silenced by VIGS, the *NbCOI1* IR plants exhibited significantly higher levels of electrolyte leakage than WT plants (Fig. 6C).

We speculated whether the enhanced virulence of PVX-PVY in *NbCOI1* IR plants compared to that in WT plants is due to increased dioxygenase activity. We analyzed dioxygenase activity in extracts of plants infected with PVX-PVY and control plants of both genotypes across time (Fig. 6E). The level of enzymatic activity was higher in mock-inoculated *NbCOI1* IR plants than in WT plants. Moreover, infection with PVX-PVY induced significantly higher dioxygenase activity in *COI1*-silenced plants than in controls at early times after infection. However, dioxygenase activity 8 days after infection with PVX-PVY was similar in WT leaves and in *NbCOI1* IR leaves. No differences were observed in plant extracts when heated at 65°C for 12 min (data not shown), a treatment that inactivated dioxygenase activity in tomato (*Solanum lycopersicum*) (51). This result further substantiates the effect

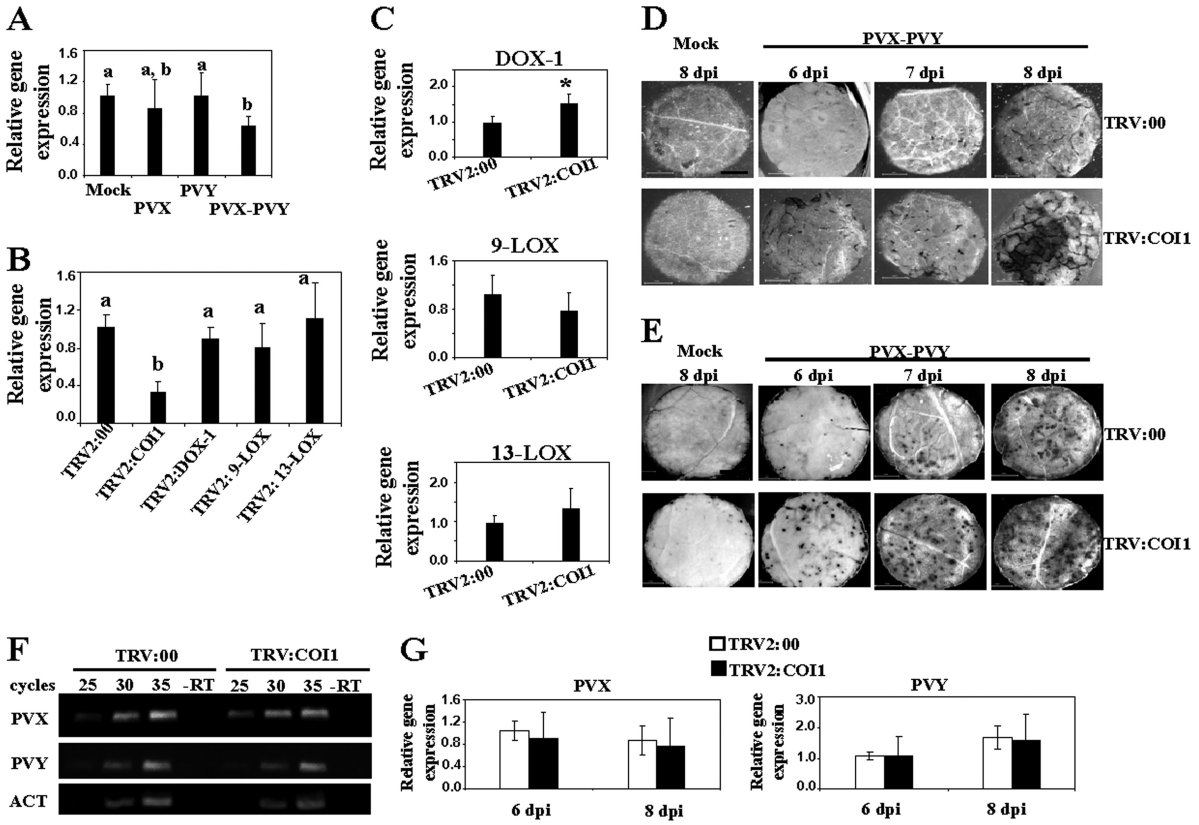

FIG 4 Silencing of *N. benthamiana COI1* results in enhanced cell death induced by PVX-PVY infection. (A) qRT-PCR analysis of expression of *COI1* in *N. benthamiana* leaves 6 days after inoculation with PVX and PVY. (B) Three-week-old *N. benthamiana* plants were infiltrated with *Agrobacterium* containing TRV2:*COI1*, TRV2:*DOX-1*, TRV2:*9-LOX*, TRV2:*13-LOX*, or TRV2:00 (vector control). qRT-PCR analysis of expression of *COI1* in silenced plants 10 days after infiltration (d.a.i.) is shown. (C) The relative expression levels of α-*DOX-1*, *13-LOX*, and *9-LOX* in *COI1*-silenced plants were estimated by qRT-PCR. Expression of the 18S rRNA gene served as a control. Data represent the means ± standard errors of three replicates, each consisting of three to five plants that received the same treatment. Statistically significant differences between means were determined by employing Duncan's multiple range test. Different letters indicate significant differences at a *P* value of 0.05. Asterisks indicate significant differences in pTRV2:*COI1*-infiltrated plants compared with nonsilenced control plants (Student's *t* test, $P = 0.05$). (D) TRV2:*COI1*- and TRV2:00-agroinfiltrated plants were mock inoculated or inoculated with PVX-PVY at 10 d.a.i. Uppermost leaves of control and *COI1*-silenced plants were stained with trypan blue to detect cell death at 6, 7, and 8 days postinoculation (d.p.i.). Scale bars = 1 mm. (E) Leaves of control and *COI1*-silenced plants were stained with NBT solution at 6, 7 and 8 d.p.i. Scale bars = 1 mm. (F) Comparison of relative viral loads estimated by RT-PCR in control and *COI1*-silenced plants at 8 d.p.i. −RT, control without RT. The same RT reactions were used to amplify actin gene transcripts as a control. (G) qRT-PCR was used to analyze the accumulation of PVX and PVY in control and *NbCOI1*-silenced plants at 6 and 8 d.p.i. Data represent the means ± standard errors.

of *COI1* silencing on the expression of oxylipin biosynthesis genes in PVX-PVY-infected plants.

We also checked the genetic interaction between *9-LOX* and *COI1* to assess whether *9-LOX* was epistatic to *COI1*. Silencing of *9-LOX* was performed by VIGS in *NbCOI1* IR and WT plants, using TRV2:00-infiltrated plants as controls (Fig. 7A). After PVX-PVY infection, the cell death-associated electrolyte leakage level in the *COI1* and *9-LOX* cosilenced plants was intermediate between those of the respective single-gene-silenced plants, and hence, this interaction was additive rather than epistatic (Fig. 7B). We then examined dioxygenase activity in these plants. Silencing of *9-LOX* compromised the increased dioxygenase activity observed in both WT and *NbCOI1* IR plants upon PVX-PVY infection (Fig. 7C). These data indicate that silencing of *9-LOX* restored to wild-type levels the enhanced virulence of PVX-PVY in *COI1*-silenced plants and, thus, that *9-LOX* is a main contributor of the dioxygenase activity elicited by PVX-PVY in *N. benthamiana*.

MeJA treatment enhances virulence of PVX-PVY. The enhanced virulence of PVX-PVY observed in the *COI1*-silenced plants suggests that repression of *COI1*-mediated signaling could enhance viral pathogenicity through oxylipin production. To determine whether the JA response affects PVX-PVY infection, we inoculated MeJA- and control-treated *N. benthamiana* plants with PVX-PVY. As expected, MeJA treatment induced the expression of the JA-dependent response genes *TD* and *proteinase inhibitor I* (Fig. 8A). The application of exogenous MeJA resulted in milder, nonnecrotic symptoms (Fig. 8B, top) and lower viral RNA accumulation (Fig. 8C) at early times postinoculation (6 d.p.i.), indicating an interference of virus infection by this hormone. Later on, MeJA-treated plants exhibited an enhanced necrosis response to PVX-PVY infection (Fig. 8B, middle). By 8 d.p.i., electrolyte leakage measurement and trypan blue staining revealed extensively enhanced cell death in MeJA-treated leaves compared with that in control-treated leaves (Fig. 9A and B). Although MeJA treatment itself induced an increase in electrolyte leakage compared to that in the control, the mock-inoculated MeJA-treated plants remained free of necrotic symptoms throughout the trial period. Virus accumulation was not affected by MeJA treatment at this

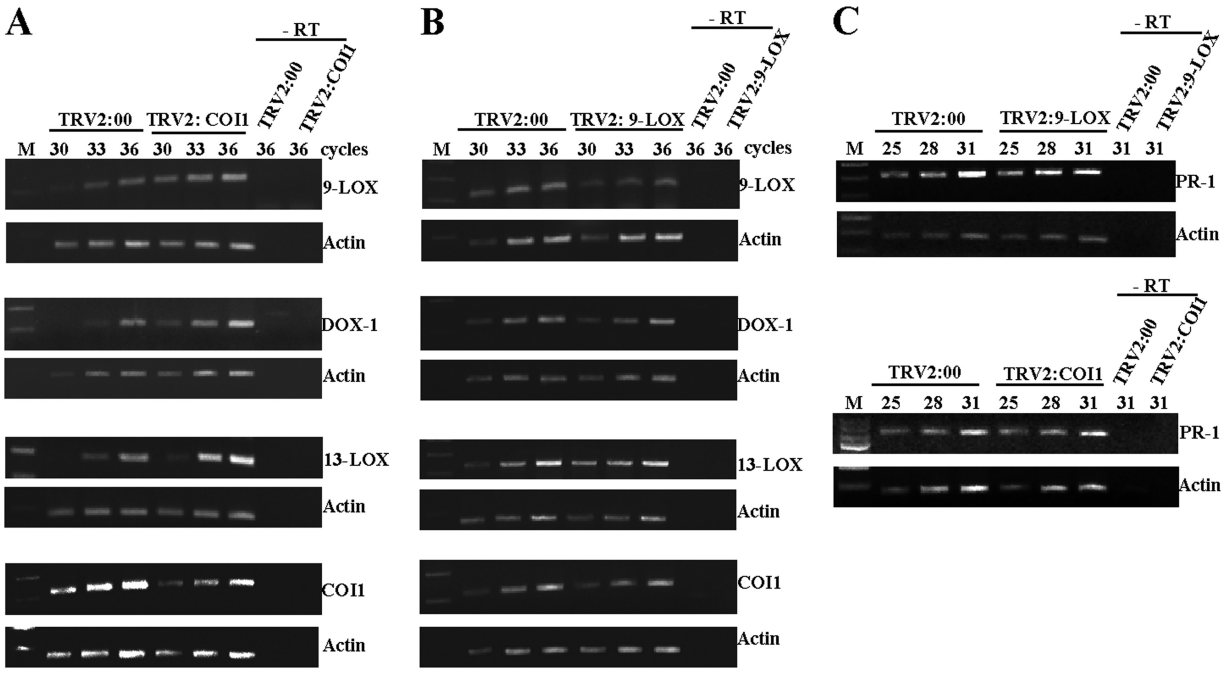

FIG 5 RT-PCR analysis of expression of the oxylipin biosynthesis and perception genes in plants infected with PVX-PVY. (A) RT-PCR analysis of expression of the *9-LOX*, α-*DOX-1*, *13-LOX*, and *COI1* genes in empty vector control (TRV2:00) and *COI1*-silenced (TRV2:*COI1*) plants 6 d.p.i. with PVX-PVY. (B) RT-PCR analysis of expression of the *9-LOX*, α-*DOX-1*, *13-LOX*, and *COI1* genes in empty vector control (TRV2:00) and *9-LOX*-silenced (TRV2:*9-LOX*) plants 8 d.p.i. with PVX and PVY. (C) RT-PCR analysis of expression of the *PR-1* gene in empty vector control (TRV2:00), *9-LOX*-silenced (TRV2:*9-LOX*) and *COI1*-silenced (TRV2:*COI1*) plants 6 d.p.i. with PVX and PVY. Experiments were repeated twice, with different sets of plants for each construct in each experiment, and obtained similar results. The same RT reactions were used to amplify actin gene transcripts as a control. The number of PCR cycles is indicated below treatments. −RT, control without RT.

late time point (Fig. 8C). Interestingly, qRT-PCR analyses showed that *13-LOX* and α-*DOX-1* gene expression was induced in MeJA-treated plants, whereas *COI1* mRNA was repressed (Fig. 9C). These results suggest a mechanistic link between the enhanced necrosis and the induction of oxylipin biosynthesis genes in MeJA-treated, PVX-PVY-infected plants. Treatment with MeJA on plants singly infected with either PVX or PVY did not result in systemic necrosis disease (data not shown).

We further tested the effects of treatments with ACC, ABA, and SA on PVX-PVY-induced necrotic symptoms (Fig. 9A). No significant effect on the extent of cell death could be attributed to treatment with ACC and ABA. Treatment with SA, however, induced a statistically significant reduction in electrolyte leakage upon virus infection. To determine whether the enhanced virulence of PVX-PVY infection in MeJA-treated plants was based on the inhibition of SA-mediated host defenses, *N. benthamiana* plants expressing the SA-degrading enzyme salicylate hydroxylase (*NahG* plants) were treated with MeJA or mock solution and then inoculated with PVX-PVY. There was no significant difference in electrolyte leakage between the infected WT and *NahG* plants with or without MeJA treatment, suggesting that the effect of SA in the necrosis response to PVX-PVY depends on the antagonistic relationship between the JA and SA signaling pathways.

Distinct responses of *NbCOI1* IR transgenic and *LOX-9*-silenced plants to *Tomato spotted wilt virus*. To determine whether oxylipins contribute to the virulence of another necrosis-inducing virus in *N. benthamiana*, we tested the levels of susceptibility of *NbCOI1* IR and *LOX-9*-silenced plants to *Tomato spotted wilt virus* (TSWV). Infection of WT plants with TSWV induced cell death, as revealed by trypan blue staining and ROS production in upper, noninoculated leaves (Fig. 10A), that led to systemic necrosis at 3 weeks postinoculation. Next, the expression levels of oxylipin biosynthesis genes were analyzed by qRT-PCR at different times postinoculation (Fig. 10B). The expression of *9-LOX*, *13-LOX*, and α-*DOX-1* mRNAs was significantly induced by TSWV from 7 d.p.i. onwards, suggesting that oxylipins may contribute to TSWV necrosis progression. In support of this hypothesis, the necrosis symptoms were delayed and the level of electrolyte leakage in the *LOX-9*-silenced plants was significantly lower than that in the nonsilenced, control plants. In contrast, infection of *NbCOI1* IR plants by TSWV caused more necrosis and higher levels of electrolyte leakage than in WT plants (Fig. 10C and D). We further investigated the effects of *9-LOX* and *COI1* silencing on the accumulation of TSWV by qRT-PCR (Fig. 10E). At 13 d.p.i., TSWV accumulation was significantly lower (2.1-fold) in the *9-LOX*-silenced plants than in the controls, whereas virus accumulated at 1.9-fold-higher levels in *NbCOI1* IR than in WT plants.

As reported above for PVX-PVY infection, MeJA treatment initially retarded the appearance of systemic symptoms but later accelerated the development of necrosis induced by TSWV infection (Fig. 11A and data not shown). The MeJA-treated, TSWV-infected plants exhibited significantly higher levels of electrolyte leakage than the control plants at late stages of infection (17 d.p.i.) (Fig. 11B). We further tested the accumulation of TSWV in MeJA- and control-treated plants at different times postinoculation. At 6 d.p.i., TSWV RNA accumulated at lower levels in MeJA-treated plants, coincident with the milder symptoms shown by the plants

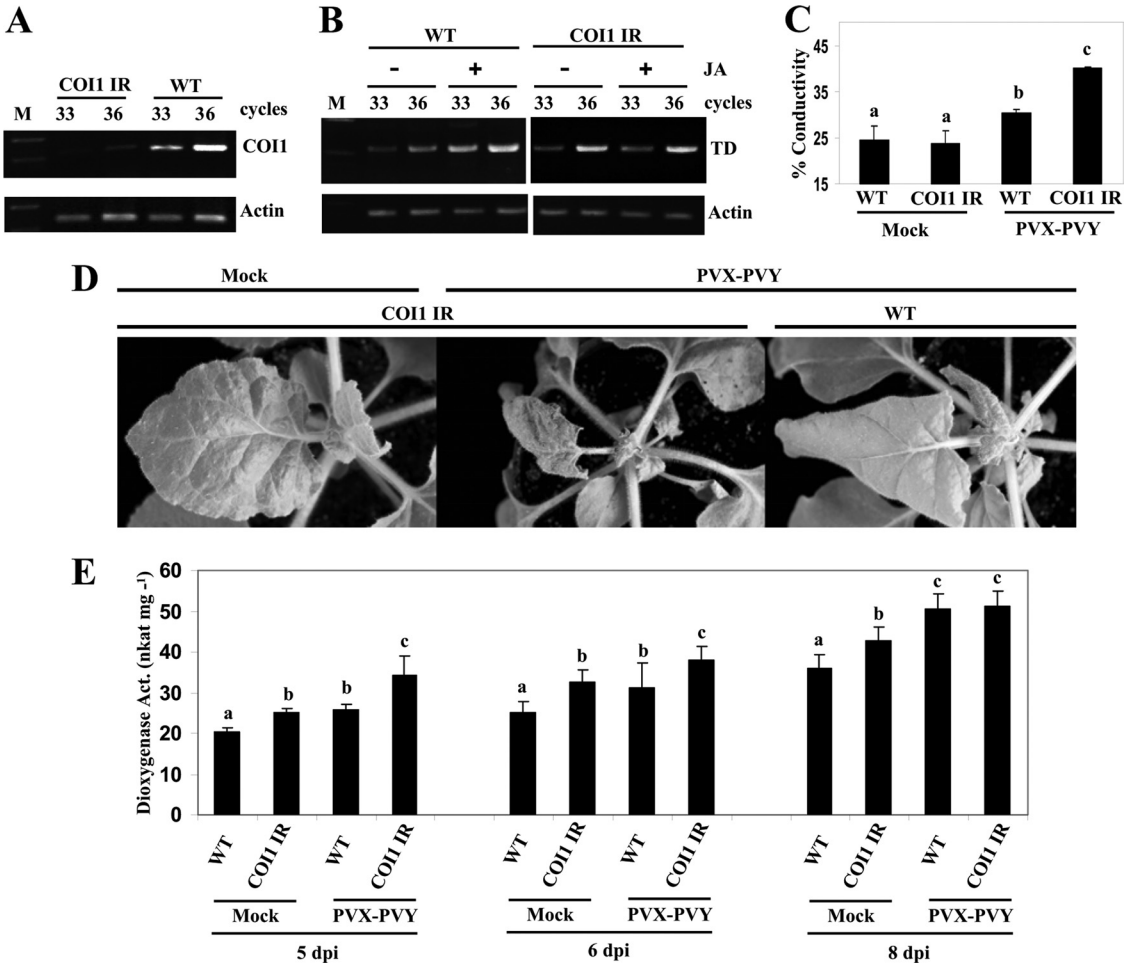

FIG 6 Enhanced virulence of PVX-PVY in *COI1*-silenced transgenic plants. (A) Silencing of *COI1* transcripts in *NbCOI1* IR line 7 was monitored by RT-PCR. (B) MeJA (JA) (250 μM) or mock solution as a control was applied to wild-type (WT) and *NbCOI1* IR plants, and the expression of *threonine deaminase* (*TD*) mRNA was monitored by RT-PCR. The same RT reactions were used to amplify actin gene transcripts as a control. (C) WT and *NbCOI1* IR plants were mock inoculated or inoculated with PVX-PVY. Leaf discs were excised and assayed for electrolyte leakage at 8 d.p.i. (D) Representative disease symptoms at 6 d.p.i. are displayed. (E) Altered dioxygenase activity (Act.) in leaf extracts from WT and *NbCOI1* IR plants that were mock inoculated or inoculated with PVX-PVY at different times postinoculation. Linoleic acid (0.1 mM) was used as a substrate. Data represent the means ± standard errors of six replicates, each consisting of three to five plants that received the same treatment in two independent experiments. Statistically significant differences between means were determined by employing Duncan's multiple range test. Different letters indicate significant differences at a *P* value of 0.05.

at early stages of infection. However, by 17 d.p.i., there was a significant increase of viral RNA in MeJA-treated plants compared to the level in controls, which correlated with the severe necrosis symptoms shown by these plants (Fig. 11C).

Attenuated susceptibility of *Arabidopsis* double *lox1* α-*dox-1* mutant to TSWV infection. To further substantiate the effects of the 9-LOX and α-DOX-1 oxylipin pathways on virus pathogenicity, we analyzed an *Arabidopsis* double mutant containing transfer DNA (T-DNA) insertions in the 9-LOX-encoding *LOX1* gene and the α-*DOX-1* gene (*lox1* α-*dox-1*) during infection with TSWV. To enhance oxylipin production, WT and *lox1* α-*dox-1* plants were also treated with MeJA and then inoculated with TSWV. Infection with TSWV induced retarded growth in WT but not in the double *lox1* α-*dox-1* mutant (Fig. 12A). Attenuated virulence of TSWV in the *lox1* α-*dox-1* mutant compared to its virulence in WT plants was also evidenced by monitoring the levels of electrolyte leakage in these plants (Fig. 12B). Furthermore, virus accumulation was attenuated in the *lox1* α-*dox-1* mutant compared with that in WT plants (Fig. 12C).

DISCUSSION

Although several studies have identified viral symptom determinants responsible for systemic necrosis, the mechanics of how they contribute to necrosis in infected plants remain poorly understood (52, 53, 54). Enhancement of several dioxygenase activities in response to fungal, bacterial, and viral pathogens appears to be a common feature occurring in several pathosystems (12). However, evidence for a potential role for oxylipins other than JA (31) in modulating virus pathogenicity in compatible interactions has not been reported before this study. Here, several oxylipin biosynthesis genes, i.e., *9-LOX*, *13-LOX*, and α-*DOX-1*, were highly expressed during compatible plant-virus interactions that led to systemic necrosis in *N. benthamiana*. Moreover, typical hallmarks of HR-type PCD (55), e.g., ROS accumulation, phenylpropanoid

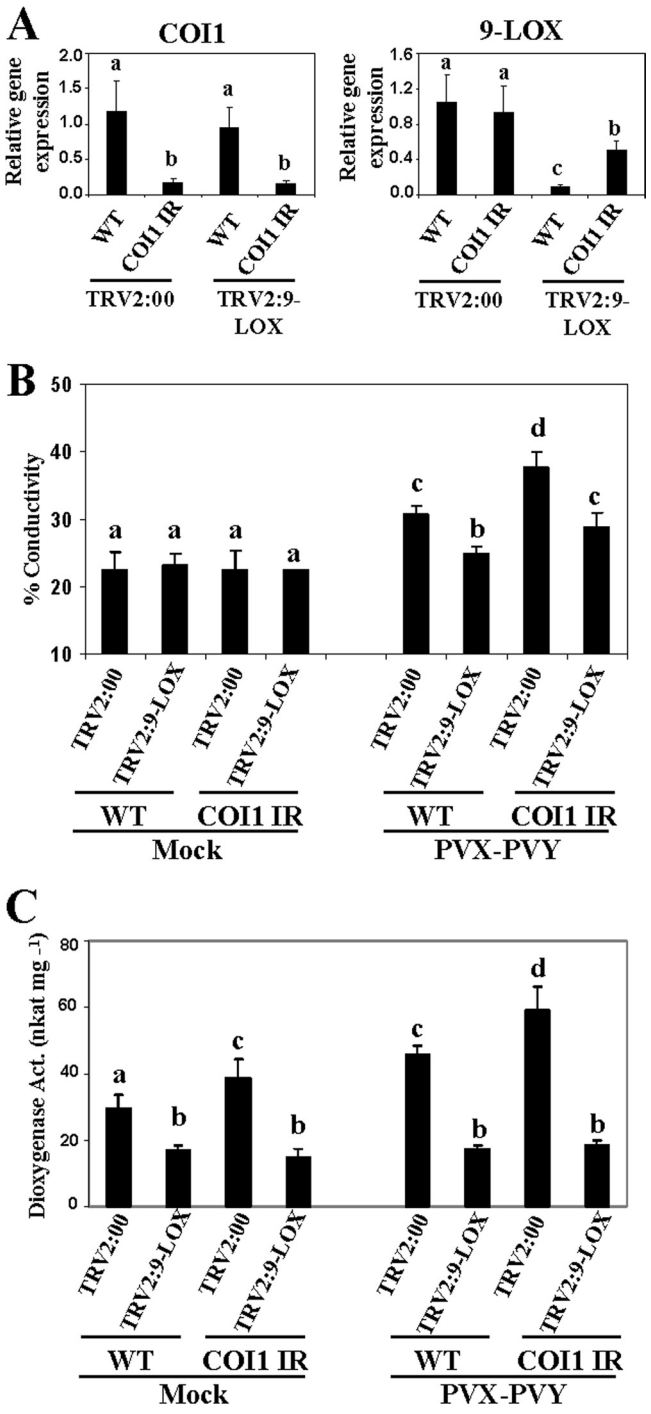

FIG 7 Effect of simultaneous silencing of *9-LOX* and *COI1* on PVX-PVY infection. *NbCOI1* IR and WT plants were infiltrated with *Agrobacterium* containing TRV2:*9-LOX* or TRV2:00 (vector control). Agroinfiltrated plants were mock inoculated or inoculated with PVX-PVY at 10 days after infiltration (d.a.i.). (A) Silencing of *COI1* and *9-LOX* transcripts was monitored by qRT-PCR in uppermost leaves at 10 d.a.i. (B) Leaf discs were excised and assayed for electrolyte leakage at 8 days postinoculation (d.p.i.). Data represent the means ± standard errors of three replicates, each consisting of three to five plants that received the same treatment. (C) Dioxygenase activity was assayed in leaf extracts at 6 d.p.i. using linoleic acid (0.1 mM) as a substrate. Data represent the means ± standard errors of six replicates, each consisting of three to five plants that received the same treatment in two independent experiments. Statistically significant differences between means were determined by employing Duncan's multiple range test. Different letters indicate significant differences at a *P* value of 0.05.

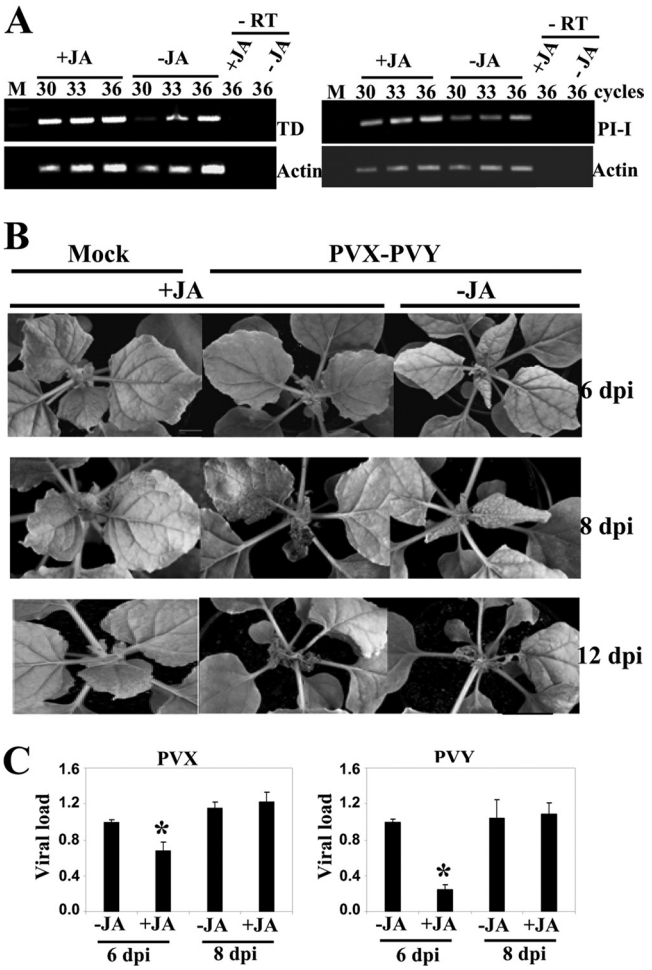

FIG 8 Effect of MeJA treatment on PVX-PVY infection. MeJA (+JA) or mock solution (−JA) as a control was applied to plants that were mock inoculated or inoculated with PVX-PVY. (A) The expression of *threonine deaminase* (*TD*) and *proteinase inhibitor I* (*PI-I*) mRNA was monitored by RT-PCR in mock-inoculated plants. The same RT reactions were used to amplify actin gene transcripts as a control. −RT, control without RT. (B) Representative disease symptoms displayed at 6, 8, and 12 d.p.i. Control plants exhibited the typical systemic symptoms associated with the viral synergistic interaction, while JA-treated plants exhibited milder symptoms at early times postinoculation (6 d.p.i.). By 8 d.p.i., MeJA-treated plants exhibited an enhanced necrosis response to PVX-PVY infection. (C) qRT-PCR was used to analyze the accumulation of PVX and PVY in plants that were treated with MeJA or mock solution and inoculated with PVX-PVY at 6 and 8 d.p.i. Data represent the means ± standard errors. Asterisks indicate significant differences in MeJA-treated plants compared with control plants at 6 d.p.i. (Student's *t* test, $P = 0.05$).

metabolites, cell membrane damage, and degradation of nuclear DNA, were also detected in plants infected by the necrosis-inducing viruses, TSWV and the synergistic pair PVX-PVY. This suggested the possibility that oxylipins might contribute to the induction of cell death responses during infection by these viral pathogens. Although the role of cell death associated with disease during biotrophic plant-virus interactions is unclear, increasing evidence suggests that disease-associated cell death is genetically controlled and is a form of PCD (10, 11, 56, 57).

Our molecular genetic study using oxylipin gene-silenced *N. benthamiana* plants revealed that enhanced expression of *9-LOX*, *13-LOX*, and α-*DOX*-1 was required for increased virulence

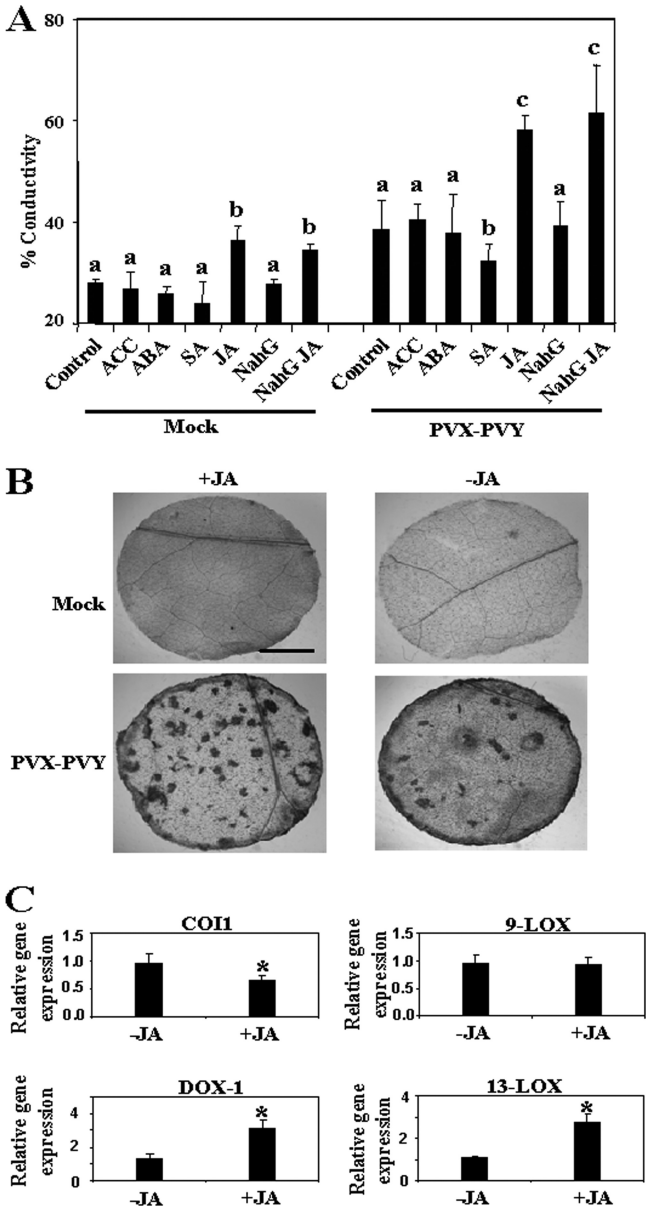

FIG 9 MeJA enhances virulence of PVX-PVY. (A) 1-Aminocyclopropane-1-carboxylic acid (ACC), abscisic acid (ABA), salicylic acid (SA), methyl jasmonate (+JA), or mock solution as a control was applied to wild-type plants that were mock inoculated or inoculated with PVX-PVY. MeJA or mock solution was applied to plants expressing the salicylate hydroxylase gene (*NahG*). Discs from uppermost leaves were excised and assayed for electrolyte leakage at 8 d.p.i. Data represent the means ± standard errors of six replicates, each consisting of three to five plants that received the same treatment. Statistical comparisons between means were made among treatments within the mock-inoculated or PVX-PVY-infected plants by employing Duncan's multiple range test. Different letters indicate significant differences at a *P* value of 0.05. (B) Uppermost leaves of control (−JA) and MeJA-treated (+JA) plants were stained with trypan blue to detect cell death at 8 d.p.i. Scale bar = 1 mm. (C) qRT-PCR analysis of expression of *COI1*, *9-LOX*, *13-LOX*, and α-*DOX-1* genes in PVX-PVY-infected plants that were treated with MeJA or mock solution. Data represent the means ± standard errors. Asterisks indicate significant differences in MeJA-treated plants compared with control plants (Student's *t* test, $P = 0.05$).

and/or cell death responses in plants infected with either TSWV or the virus pair PVX-PVY. In contrast to the phenotypes that occurred with reduced expression of oxylipins, *COI1*-silenced plants exhibited enhanced susceptibility to virus infection, which was accompanied by an increased expression of *9-LOX*, *13-LOX*, and α-*DOX-1* in these plants. Importantly, dioxygenase activity also increased rapidly and to a higher level in *NbCOI1* IR plants infected by PVX-PVY just before the onset of the necrosis response. Thus, oxylipin biosynthesis genes function as virulence factors during compatible virus infections that cause systemic necrosis. Silencing of any of the three branches of the oxylipin pathway negatively affected the systemic necrosis caused by PVX-PVY. However, the 9-LOX branch seemed to be a major contributor, since (i) silencing of *9-LOX* restored to wild-type levels the enhanced virulence of PVX-PVY in *COI1*-silenced plants and (ii) silencing of *9-LOX* compromised the increased dioxygenase activity observed in both WT and *NbCOI1* IR plants upon PVX-PVY infection. This was consistent with studies reporting the massive accumulation of 9-LOX derivatives in the HR elicited in *N. tabacum* by *Tobacco mosaic virus*, which represented about 95% of the total lipid peroxides (58). The hypothesis that oxylipins contribute to modulation of pathogenesis in compatible interactions is supported by previous findings. In maize (*Zea mays*), a plant 9-LOX activity served as a fungal susceptibility factor through stimulation of mycotoxin production and conidium formation (18). Thatcher and associates (59) reported that *Fusarium oxysporum* hijacked nondefensive roles of the JA-signaling pathway to cause wilt disease symptoms that led to plant death in *Arabidopsis*.

Lipid peroxidation is an important feature of HR-type PCD during incompatible or nonhost interactions of plants with pathogens. In particular, the production of free fatty acid hydroperoxides via the 9-LOX pathway has been proposed to be involved in the HR of tobacco induced by the avirulent pathogen *Pseudomonas syringae* pv. *syringae* (60) and by cryptogein, an elicitor from *Phytophthora cryptogea* (24). In addition, a role of several oxylipins, originating from 13-LOX activities, in promoting localized cell death during the HR has also been reported in different pathosystems (24, 25, 61). LOX activities were suggested to participate in membrane degradation at the sites of infection by generation of highly reactive molecules, such as hydroperoxides, alkenals, and aldehydes, and thus contribute to hypersensitive cell death (24). Recent genetic studies, however, indicate that diverse oxylipins might impart novel signaling activities in their own right during plant defense, as is the case for prostaglandins in animals (15, 62). In this study, we have shown that oxylipins are involved as effectors and/or as signaling components in the process of PCD induced by both PVX-PVY-associated synergism and TSWV in *N. benthamiana*. Thus, oxylipin metabolism is proposed to be implicated not only in the HR-associated resistance response against bacteria and fungi but also in systemic necrosis disease induced by compatible plant-virus interactions. The existence of common signaling components during HR and disease-associated cell death is also supported by previous findings. Komatsu et al. (10) determined that *SGT1* and *RAR1*, as well as components of the mitogen-activated protein kinase (MAPK) cascade, were essential for PCD in both *Rx*-mediated HR to PVX and the systemic necrosis induced by *Plantago asiatica mosaic virus* (PlAMV) in *N. benthamiana*. In addition, del Pozo et al. (63) identified a MAP kinase kinase kinase gene (*MAPKKK*α) that positively regulates cell

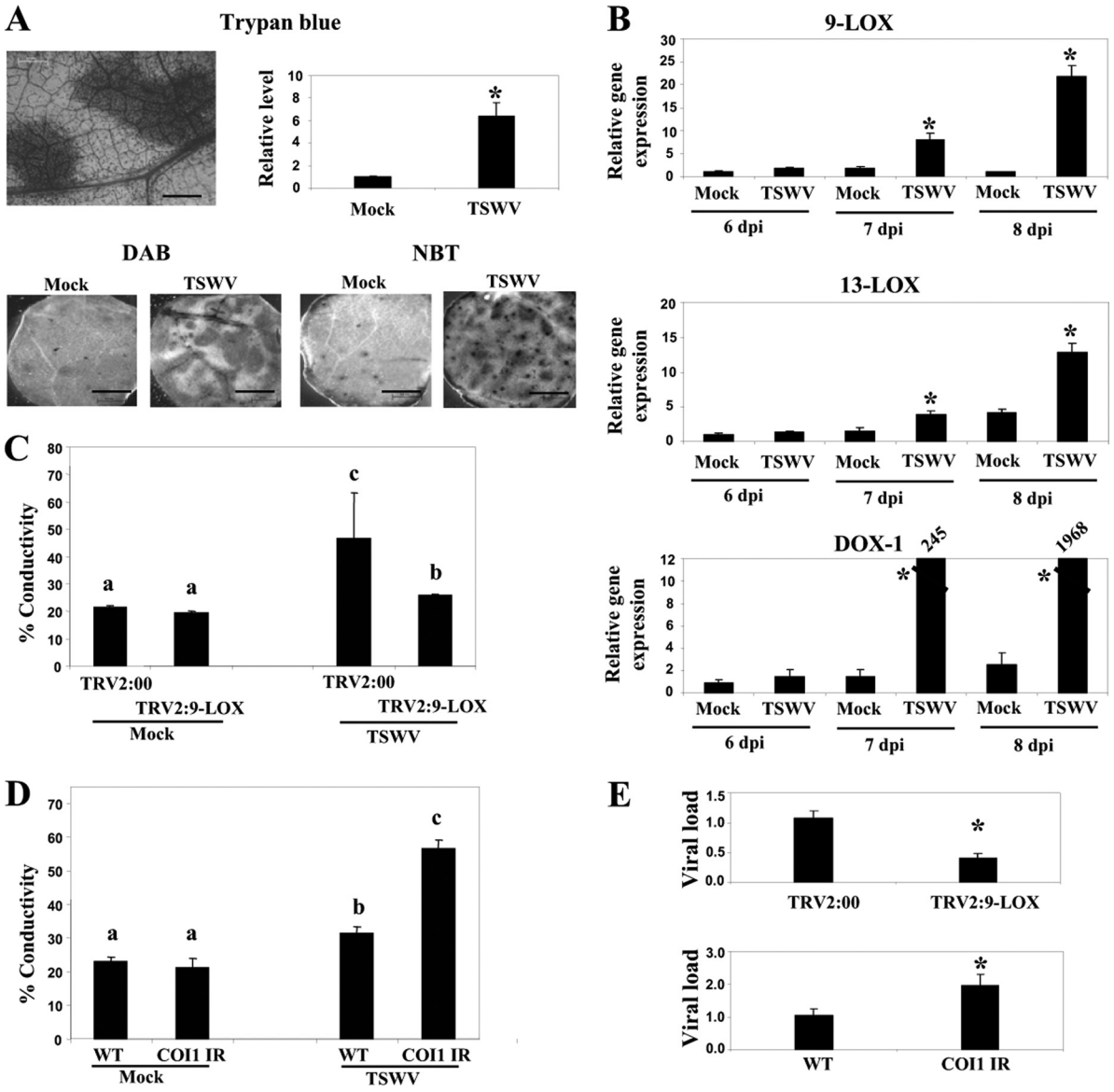

FIG 10 Effect of *9-LOX* and *COI1* silencing on TSWV infection (A, top) Uppermost leaves of control and TSWV-infected plants were stained with trypan blue to detect cell death at 9 d.p.i. Scale bars = 0.2 mm. The absorbance of the dye was measured spectrophotometrically at 590 nm. (Bottom) Leaf discs were stained with either DAB or NBT solution to monitor ROS production. Scale bars = 1 mm. (B) The relative expression levels of *9-LOX*, *13-LOX*, and α-*DOX-1* in mock-inoculated plants and plants infected with TSWV at 6, 7 and 8 d.p.i. were estimated by qRT-PCR. Asterisks indicate significant differences in TSWV-infected plants compared with control plants (Student's *t* test, $P = 0.05$). (C) Plants were infiltrated with *Agrobacterium* containing TRV2:*9-LOX* or TRV2:00 (vector control). Agroinfiltrated plants were mock inoculated or inoculated with TSWV at 10 days after infiltration. Leaf discs were excised and assayed for electrolyte leakage at 13 d.p.i. (D) WT and *NbCOI1* IR plants were mock inoculated or inoculated with TSWV. Leaf discs were excised and assayed for electrolyte leakage at 13 d.p.i. (E) qRT-PCR was used to analyze the accumulation of TSWV in *NbCOI1* IR and *9-LOX*-silenced plants compared to the level in control plants at 13 d.p.i.

death associated with both HR-type resistance and disease in plants undergoing *P. syringae* infection.

The enhanced virulence of both TSWV and PVX-PVY in *COI1*-silenced plants was mimicked by treatment of WT plants with MeJA, which was correlated with an increased expression of genes encoding oxylipin biosynthesis, *13-LOX* and α-*DOX-1*. This response was independent from SA-dependent defenses, as *NahG* plants showed disease susceptibility similar to that of WT plants whether treated with MeJA or not. The participation of JA in the signaling cascade leading to oxylipin gene expression has been previously documented. Induction of α-*DOX-1* was observed in *N. attenuata* after the application of MeJA (64). Moreover, treatment of cotton (*Gossypium hirsutum*) with MeJA induced both 9- and 13-LOX activities, as well as transcription of its *LOX1*, illustrating a positive regulation of these branches of the oxylipin pathway by JA. Interestingly, HR-like symptoms were observed in cotton when a compatible *Xanthomonas campestris* pv. *malvacearum* strain was inoculated onto MeJA-treated cotyledons (27). This may indicate the potential of compatible interactions to trigger PCD responses provided that certain threshold levels of oxylipins accumulate during infection.

We also investigated the effect of oxylipins on virus multipli-

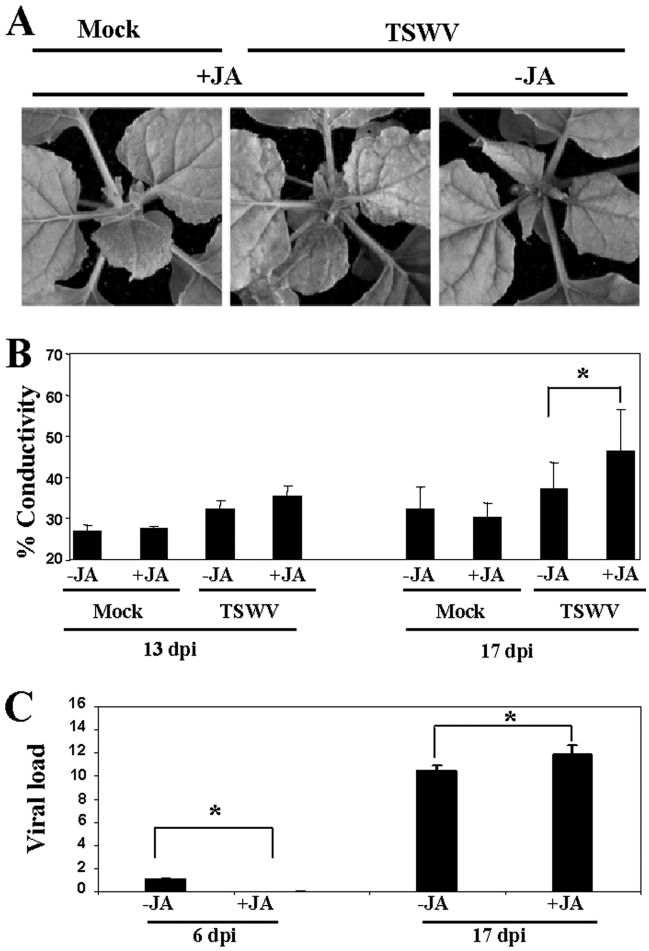

FIG 11 MeJA enhances virulence of TSWV. (A) MeJA (+JA) or mock solution (−JA) as a control was applied to plants that were mock inoculated or inoculated with TSWV. Representative disease symptoms at 17 d.p.i. are displayed. (B) Leaf discs were excised and assayed for electrolyte leakage at 13 and 17 d.p.i. Asterisks indicate significant differences in MeJA-treated plants compared with control plants (Student's *t* test, $P = 0.05$). Data represent the means ± standard errors of three replicates, each consisting of three to five plants that received the same treatment. Statistically significant differences between means were determined by employing Duncan's multiple range test. Different letters indicate significant differences at $P = 0.05$. (C) qRT-PCR was used to analyze the accumulation of TSWV in plants that were treated with MeJA or mock solution and inoculated with TSWV at 6 and 17 d.p.i. Data represent the means ± standard errors. Asterisks indicate significant differences in MeJA-treated plants compared with control plants (Student's *t* test, $P = 0.05$).

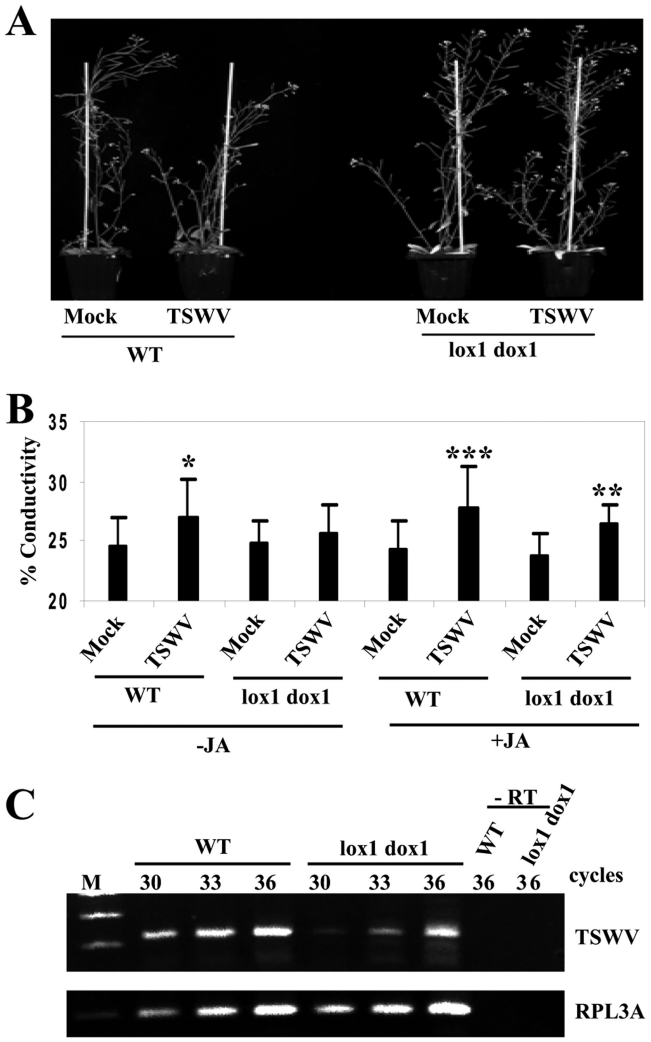

FIG 12 Attenuated susceptibility of *Arabidopsis* double *lox1* α-*dox-1* mutant to TSWV infection. (A) *Arabidopsis lox1* α-*dox-1* double mutant and WT plants were mock inoculated or inoculated with TSWV. Representative disease symptoms at 17 d.p.i. are displayed. (B) Leaf discs were excised and assayed for electrolyte leakage at 17 d.p.i. Asterisks indicate significant differences in TSWV-inoculated plants compared with control plants (Student's *t* test: *, $P = 0.1$; **, $P = 0.05$; ***, $P = 0.01$). Data represent the means ± standard errors of eight replicates, each consisting of six plants that received the same treatment. (C) Comparison of relative viral loads estimated by RT-PCR in WT and *lox1* α-*dox-1* mutant plants at 17 d.p.i. −RT, control without RT. The same RT reactions were used to amplify RPL3A gene transcripts as a control.

cation in systemic necrosis. Both PVX and PVY accumulated to similar levels in oxylipin-silenced plants compared to their levels in nonsilenced plants, suggesting that multiplication of the synergistic pair was not restrained by disease-associated cell death in this pathosystem. Accordingly, the acceleration of cell death caused by the silencing of *COI1* did not inhibit the accumulation of the viruses. In contrast, silencing of *9-LOX* in *N. benthamiana* or knockout of both *9-LOX* and α-*DOX-1* genes in *A. thaliana* had a negative impact on TSWV accumulation. How oxylipin metabolism can enhance TSWV accumulation is presently unknown. Nevertheless, our results resemble the earlier observation that PCD may not play a primary role in restraining virus accumulation in HR-type resistance (65). Interestingly, it has been reported that restraint of virus accumulation was induced in the systemic necrosis caused by PlAMV through pathways distinct from those leading to PCD (10). This partial restraint required *SGT1* and *RAR1* but not the MAPK cascade involving *MAPKKK*α and *MEK2*. Thus, it is tempting to speculate that oxylipin biosynthesis genes might be operating in the MAPK cascade that leads to disease-associated cell death but not in restraining the accumulation of necrosis-inducing viruses.

It has been suggested that symptoms in potyvirus-infected plants are associated at least to some extent with the RNA-silencing suppressor activity of the HC-Pro protein that interferes with endogenous microRNA (miRNA) accumulation, causes misregulation of the expression of several miRNA-regulated transcription

factors, and produces developmental defects in transgenic plants (66). Similarly, transgenic expression of the silencing suppressor protein of PVX, P25, produced developmental alterations in *N. benthamiana* (67). Thus, PVX-PVY-associated synergism could partly be caused by the combined effect of both suppressors on several RNA-regulated networks. Indeed, our previous studies revealed that double infection by PVX and PVY altered the accumulation of miRNAs and their target transcripts to a greater extent than single infections (68). Interestingly, it has been reported that miR319-targeted *TCP* (*TEOSINTE BRANCHED/CYCLOIDEA/PCF*) transcription factors positively regulate leaf senescence, a type of PCD, in *Arabidopsis thaliana* via modulation of *LOX2* and the oxylipin biosynthesis pathway (69). Thus, it is plausible that a disturbed, miRNA-based regulation contributes to systemic necrosis caused by PVX-PVY infection via oxylipin production. This observation is consistent with a report showing the upregulation of *TCP1* and *LOX2* in tomato plants infected with *Groundnut bud necrosis tospovirus*, which might be responsible for the systemic necrosis exhibited by these plants (70).

To summarize, our findings provide compelling evidence that oxylipins may be positive regulators of cell death responses induced by compatible virus infections that lead to systemic necrosis. Therefore, we propose a common role for oxylipins as a shared signaling component of cell death during both compatible and incompatible plant-pathogen interactions. Further investigations must be focused on addressing the involvement of oxylipins in other viral infections associated with systemic necrosis diseases.

ACKNOWLEDGMENTS

A.G.-M. was the recipient of a CSIC JAE-Doc contract from the program Junta para la Ampliación de Estudios, cofunded by the European Social Funds. R.P. was the recipient of a contract from the CSIC. This work was supported by grant BIO2009-10172 from the Spanish Ministry of Science and Innovation.

We thank C. Castresana (Centro Nacional de Biotecnología, Spain) for providing *A. thaliana lox1* α*-dox-1* mutant, H.-S. Guo (Chinese Academy of Sciences, China) for providing *NahG N. benthamiana* plants, E. Moriones (Instituto de Hortofruticultura Subtropical y Mediterránea, Spain) for providing the TSWV strain TM-1, and T. Canto (Centro de Investigaciones Biológicas, Spain) for critically reading the manuscript.

We declare no conflicts of interest.

REFERENCES

1. **Culver JN, Padmanabhan MS.** 2007. Virus-induced disease: altering host physiology one interaction at a time. Annu. Rev. Phytopathol. **45**:221–243.
2. **Pallas V, García JA.** 2011. How do plant viruses induce disease? Interactions and interference with host components. J. Gen. Virol. **92**:2691–2705.
3. **Whitham SA, Yang C, Goodin M.** 2006. Global impact: elucidating plant responses to viral infection. Mol. Plant Microbe Interact. **19**:1207–1215.
4. **Hanssen IM, van Esse HP, Ballester AR, Hogewoning SW, Parra NO, Paeleman A, Lievens B, Bovy AG, Thomma BP.** 2011. Differential tomato transcriptomic responses induced by pepino mosaic virus isolates with differential aggressiveness. Plant Physiol. **156**:301–318.
5. **Huang Z, Yeakley JM, Garcia EW, Holdridge JD, Fan JB, Whitham SA.** 2005. Salicylic acid-dependent expression of host genes in compatible Arabidopsis-virus interactions. Plant Physiol. **137**:1147–1159.
6. **Inaba J, Kim BM, Shimura H, Masuta C.** 2011. Virus-induced necrosis is a consequence of direct protein-protein interaction between a viral RNA-silencing suppressor and a host catalase. Plant Physiol. **156**:2026–2036.
7. **Satoh K, Shimizu T, Kondoh H, Hiraguri A, Sasaya T, Choi IR, Omura T, Kikuchi S.** 2001. Relationship between symptoms and gene expression induced by the infection of three strains of *Rice dwarf virus*. PLoS One **6**:e18094. doi:10.1371/journal.pone.0018094.
8. **Kim B, Masuta C, Matsuura H, Takahashi H, Inukai T.** 2008. Veinal necrosis induced by *Turnip mosaic virus* infection in *Arabidopsis* is a form of defense response accompanying HR-like cell death. Mol. Plant Microbe Interact. **21**:260–268.
9. **Garcia-Marcos A, Pacheco R, Martiáñez J, González-Jara P, Díaz-Ruíz JR, Tenllado F.** 2009. Transcriptional changes and oxidative stress associated with the synergistic interaction between *Potato virus X* and *Potato virus Y* and their relationship with symptom expression. Mol. Plant Microbe Interact. **22**:1431–1444.
10. **Komatsu K, Hashimoto M, Ozeki J, Yamaji Y, Maejima K, Senshu H, Himeno M, Okano Y, Kagiwada S, Namba S.** 2010. Viral-induced systemic necrosis in plants involves both programmed cell death and the inhibition of viral multiplication, which are regulated by independent pathways. Mol. Plant Microbe Interact. **23**:283–293.
11. **Xu P, Roossinck MJ.** 2000. *Cucumber mosaic virus* D satellite RNA-induced programmed cell death in tomato. Plant Cell **12**:1079–1092.
12. **Blée E.** 2002. Impact of phyto-oxylipins in plant defense. Trends Plant Sci. **7**:315–321.
13. **Andreou A, Brodhun F, Feussner I.** 2009. Biosynthesis of oxylipins in non-mammals. Prog. Lipid Res. **48**:148–170.
14. **Mueller MJ, Berger S.** 2009. Reactive electrophilic oxylipins: pattern recognition and signalling. Phytochemistry **70**:1511–1521.
15. **Howe GA, Schilmiller AL.** 2002. Oxylipin metabolism in response to stress. Curr. Opin. Plant Biol. **5**:230–236.
16. **Wu J, Baldwin IT.** 2010. New insights into plant responses to the attack from insect herbivores. Annu. Rev. Genet. **44**:1–24.
17. **Chini A, Boter M, Solano R.** 2009. Plant oxylipins: COI1/JAZs/MYC2 as the core jasmonic acid-signalling module. FEBS J. **276**:4682–4692.
18. **Gao X, Starr J, Gobel C, Engelberth J, Feussner I, Tumlinson J, Kolomiets M.** 2008. Maize 9-lipoxygenase ZmLOX3 controls development, root-specific expression of defense genes, and resistance to root-knot nematodes. Mol. Plant Microbe Interact. **21**:98–109.
19. **Vellosillo T, Martínez M, López MA, Vicente J, Cascón T, Dolan L, Hamberg M, Castresana C.** 2007. Oxylipins produced by the 9-lipoxygenase pathway in *Arabidopsis* regulate lateral root development and defense responses through a specific signaling cascade. Plant Cell **19**:831–846.
20. **De León IP, Sanz A, Hamberg M, Castresana C.** 2002. Involvement of the *Arabidopsis* α-DOX1 fatty acid dioxygenase in protection against oxidative stress and cell death. Plant J. **29**:61–72.
21. **Hamberg M, Sanz A, Rodriguez MJ, Calvo AP, Castresana C.** 2003. Activation of the fatty acid α-dioxygenase pathway during bacterial infection of tobacco leaves. Formation of oxylipins protecting against cell death. J. Biol. Chem. **278**:51796–51805.
22. **Rancé I, Fournier J, Esquerré-Tugayé MT.** 1998. The incompatible interaction between *Phytophthora parasitica* var. *nicotianae* race 0 and tobacco is suppressed in transgenic plants expressing antisense lipoxygenase sequences. Proc. Natl. Acad. Sci. U. S. A. **95**:6554–6559.
23. **Vicente J, Cascón T, Vicedo B, García-Agustín P, Hamberg M, Castresana C.** 2012. Role of 9-lipoxygenase and α-dioxygenase oxylipin pathways as modulators of local and systemic defense. Mol. Plant. **5**:914–928.
24. **Rustérucci C, Montillet JL, Agnel JP, Battesti C, Alonso B, Knoll A, Bessoule JJ, Etienne P, Suty L, Blein JL, Triantaphylides C.** 1999. Involvement of lipoxygenase-dependent production of fatty acid hydroperoxides in the development of the hypersensitive cell death induced by cryptogein on tobacco leaves. J. Biol. Chem. **274**:36446–36455.
25. **Vollenweider S, Weber H, Stolz S, Chételat A, Farmer EE.** 2000. Fatty acid ketodienes and fatty acid ketotrienes: Michael addition acceptors that accumulate in wounded and diseased *Arabidopsis* leaves. Plant J. **24**:467–476.
26. **Cacas JL, Vailleau F, Davoine C, Ennar N, Agnel JP, Tronchet M, Ponchet M, Blein JP, Roby D, Triantaphylides C, Montillet JL.** 2005. The combined action of 9 lipoxygenase and galactolipase is sufficient to bring about programmed cell death during tobacco hypersensitive response. Plant Cell Environ. **28**:1367–1378.
27. **Marmey P, Jalloul A, Alhamdia M, Assigbetse K, Cacas JL, Voloudakis AE, Champion A, Clerivet A, Montillet JL, Nicole M.** 2007. The 9-lipoxygenase GhLOX1 gene is associated with the hypersensitive reaction of cotton *Gossypium hirsutum* to *Xanthomonas campestris* pv. *malvacearum*. Plant Physiol. Biochem. **45**:596–606.
28. **Kovac M, Müller A, Milanovic-Jarh D, Milavec M, Düchting P, Ravnikar M.** 2009. Multiple hormone analysis indicates involvement of jasmonate signalling in the early defence of potato to *Potato virus* Y^{NTN}. Biol. Plant. **53**:195–199.
29. **Gullner G, Künstler A, Király L, Pogány M, Tobia I.** 2010. Up-regulated

expression of lipoxygenase and divinyl ether synthase genes in pepper leaves inoculated with Tobamoviruses. Physiol. Mol. Plant Pathol. **74**:387–393.
30. **Jameson PE, Clarke SF.** 2002. Hormone-virus interactions in plants. Crit. Rev. Plant Sci. **21**:205–228.
31. **Shang J, Xi DH, Xu F, Wang SD, Cao S, Xu MY, Zhao PP, Wang JH, Jia SD, Zhang ZW, Yuan S, Lin HH.** 2011. A broad-spectrum, efficient and nontransgenic approach to control plant viruses by application of salicylic acid and jasmonic acid. Planta **233**:299–308.
32. **Lozano-Duran R, Rosas-Diaz T, Gusmaroli G, Luna AP, Taconnat L, Deng XW, Bejarano ER.** 2011. Geminiviruses subvert ubiquitination by altering CSN-mediated derubylation of SCF E3 ligase complexes and inhibit jasmonate signaling in Arabidopsis thaliana. Plant Cell **23**:1014–1032.
33. **González-Jara P, Tenllado F, Martínez-García B, Atencio FA, Barajas D, Vargas M, Díaz-Ruiz J, Díaz-Ruiz JR.** 2004. Host-dependent differences during synergistic infection by Potyviruses with potato virus X. Mol. Plant Pathol. **5**:29–35.
34. **Ying XB, Dong L, Zhu H, Duan CG, Du QS, Lv DQ, Fang YY, Garcia JA, Fang RX, Guo HS.** 2010. RNA-dependent RNA polymerase 1 from *Nicotiana tabacum* suppresses RNA silencing and enhances viral infection in *Nicotiana benthamiana*. Plant Cell **22**:1358–1372.
35. **Thordal-Christensen H, Zhang Z, Wei Y, Collinge DB.** 1997. Subcellular localization of H_2O_2 in plants. H_2O_2 accumulation in papillae and hypersensitive response during the barley-powdery mildew interaction. Plant J. **11**:1187–1194.
36. **Díaz-Vivancos P, Clemente-Moreno MJ, Rubio M, Olmos E, García JA, Martínez-Gómez P, Hernández JA.** 2008. Alteration in the chloroplastic metabolism leads to ROS accumulation in pea plants in response to *Plum pox virus*. J. Exp. Bot. **59**:2147–2160.
37. **Dietrich RA, Delaney TP, Uknes SJ, Ward ER, Ryals JA, Dangl JL.** 1994. *Arabidopsis* mutants simulating disease resistance response. Cell **77**:565–577.
38. **Pacheco R, García-Marcos A, Manzano A, García de Lacoba M, Camañes G, García-Agustín P, Díaz-Ruíz JR, Tenllado F.** 2012. Comparative analysis of transcriptomic and hormonal responses to compatible and incompatible plant-virus interactions that lead to cell death. Mol. Plant Microbe Interact. **25**:709–723.
39. **Liu Y, Schiff M, Dinesh-Kumar SP.** 2004. Involvement of MEK1 MAPKK, NTF6 MAPK, WRKY/MYB transcription factors, COI1 and CTR1 in *N*-mediated resistance to *Tobacco mosaic virus*. Plant J. **38**:800–809.
40. **Tenllado F, Díaz-Ruíz JR.** 2001. Double-stranded RNA-mediated interference with plant virus infection. J. Virol. **75**:12288–12297.
41. **Karimi M, Inze D, Depicker A.** 2002. GATEWAY vectors for Agrobacterium-mediated plant transformation. Trends Plant Sci. **7**:193–195.
42. **Bradford M.** 1976. A rapid and sensitive method for the quantitation of microgram quantities of protein utilizing the principle of protein-dye binding. Anal. Biochem. **72**:248–254.
43. **Hwang IS, Hwang BK.** 2010. The pepper 9-lipoxygenase gene CaLOX1 functions in defense and cell death responses to microbial pathogens. Plant Physiol. **152**:948–967.
44. **Dixon RA, Paiva NL.** 1995. Stress-induced phenylpropanoid metabolism. Plant Cell **7**:1085–1097.
45. **Gavrieli Y, Sherman Y, Ben-Sasson SA.** 1992. Identification of programmed cell death in situ via specific labeling of nuclear DNA fragmentation. J. Cell Biol. **119**:493–501.
46. **Bannenberg G, Martínez M, Hamberg M, Castresana C.** 2009. Diversity of the enzymatic activity in the lipoxygenase gene family of Arabidopsis thaliana. Lipids **44**:85–95.
47. **Halitschke R, Baldwin IT.** 2003. Antisense LOX expression increases herbivore performance by decreasing defense responses and inhibiting growth-related transcriptional reorganization in *Nicotiana attenuata*. Plant J. **36**:794–807.
48. **Sanz A, Moreno JI, Castresana C.** 1998. PIOX, a new pathogen-induced oxygenase with homology to animal cyclooxygenase. Plant Cell **10**:1523–1537.
49. **Paschold A, Halitschke R, Baldwin IT.** 2007. Co(i)-ordinating defenses: NaCOI1 mediates herbivore-induced resistance in *Nicotiana attenuata* and reveals the role of herbivore movement in avoiding defenses. Plant J. **51**:79–91.
50. **Kang JH, Wang L, Giri A, Baldwin IT.** 2006. Silencing threonine deaminase and JAR4 in *Nicotiana attenuata* impairs jasmonic acid-isoleucine-mediated defenses against *Manduca sexta*. Plant Cell **18**:3303–3320.
51. **Rodrigo D, Jolie R, Van Loey A.** 2007. Thermal and high pressure stability of tomato lipoxygenase and hydroperoxide lyase. J. Food Eng. **79**:423–429.
52. **Király L, Cole AB, Bourque JE, Schoelz JE.** 1999. Systemic cell death is elicited by the interaction of a single gene in *Nicotiana clevelandii* and gene VI of *Cauliflower mosaic virus*. Mol. Plant Microbe Interact. **12**:919–925.
53. **Burgyán J, Hornyik C, Szittya G, Silhavy D, Bisztray G.** 2000. The ORF1 products of tombusviruses play a crucial role in lethal necrosis of virus-infected plants. J. Virol. **74**:10873–10881.
54. **Komatsu K, Hashimoto M, Maejima K, Shiraishi T, Neriya Y, Miura C, Minato N, Okano Y, Sugawara K, Yamaji Y, Namba S.** 2011. A necrosis-inducing elicitor domain encoded by both symptomatic and asymptomatic *Plantago asiatica mosaic virus* isolates, whose expression is modulated by virus replication. Mol. Plant Microbe Interact. **24**:408–420.
55. **Lam E, Kato N, Lawton M.** 2001. Programmed cell death, mitochondria and the plant hypersensitive response. Nature **411**:848–853.
56. **Atsumi G, Kagaya U, Kitazawa H, Nakahara KS, Uyeda I.** 2009. Activation of the salicylic acid signaling pathway enhances *Clover yellow vein virus* virulence in susceptible pea cultivars. Mol. Plant Microbe Interact. **22**:166–175.
57. **Kim BM, Suehiro N, Natsuaki T, Inukai T, Masuta C.** 2010. The P3 protein of *Turnip mosaic virus* can alone induce hypersensitive response-like cell death in *Arabidopsis thaliana* carrying TuNI. Mol. Plant Microbe Interact. **23**:144–152.
58. **Montillet JL, Agne JP, Ponchet M, Vailleau F, Roby D, Triantaphylides C.** 2002. Lipoxygenase-mediated production of fatty acid hydroperoxides is a specific signature of the hypersensitive reaction in plants. Plant Physiol. Biochem. **40**:633–639.
59. **Thatcher LF, Manners JM, Kazan K.** 2009. *Fusarium oxysporum* hijacks COI1-mediated jasmonate signaling to promote disease development in *Arabidopsis*. Plant J. **58**:927–939.
60. **Montillet JL, Chamnongpol S, Rusterucci C, Dat J, van de Cotte B, Agnel JP, Battesti C, Inze D, Van Breusegem F, Triantaphylides C.** 2005. Fatty acid hydroperoxides and H_2O_2 in the execution of hypersensitive cell death in tobacco leaves. Plant Physiol. **138**:1516–1526.
61. **Davoine C, Falletti O, Douki T, Iacazio G, Ennar N, Montillet JL, Triantaphylides C.** 2006. Adducts of oxylipin electrophiles to glutathione reflect a 13 specificity of the downstream lipoxygenase pathway in the tobacco hypersensitive response. Plant Physiol. **140**:1484–1493.
62. **Noverr MC, Erb-Downward JR, Huffnagle GB.** 2003. Production of eicosanoids and other oxylipins by pathogenic eukaryotic microbes. Clin. Microbiol. Rev. **16**:517–533.
63. **del Pozo O, Pedley KF, Martin GB.** 2004. MAPKKKα is a positive regulator of cell death associated with both plant immunity and disease. EMBO J. **23**:3072–3082.
64. **Paschold A, Bonaventure G, Kant MR, Baldwin IT.** 2008. Jasmonate perception regulates jasmonate biosynthesis and JA-Ile metabolism: the case of COI1 in *Nicotiana attenuata*. Plant Cell Physiol. **49**:1165–1175.
65. **Soosaar JL, Burch-Smith TM, Dinesh-Kumar SP.** 2005. Mechanisms of plant resistance to viruses. Nat. Rev. Microbiol. **3**:789–798.
66. **Kasschau KD, Xie Z, Allen E, Llave C, Chapman EJ, Krizan KA, Carrington JC.** 2003. P1/HC-Pro, a viral suppressor of RNA silencing, interferes with *Arabidopsis* development and miRNA function. Dev. Cell **4**:205–217.
67. **Siddiqui SA, Sarmiento C, Truve E, Lehto H, Lehto K.** 2008. Phenotypes and functional effects caused by various viral RNA silencing suppressors in transgenic *Nicotiana benthamiana* and *N. tabacum*. Mol. Plant Microbe Interact. **21**:178–187.
68. **Pacheco R, García-Marcos A, Barajas D, Martiáñez J, Tenllado F.** 2012. PVX-potyvirus synergistic infections differentially alter microRNA accumulation in *Nicotiana benthamiana*. Virus Res. **165**:231–235.
69. **Schommer C, Palatnik JF, Aggarwal P, Chételat A, Cubas P, Farmer EE, Nath U, Weigel D.** 2008. Control of jasmonate biosynthesis and senescence by miR319 targets. PLoS Biol. **6**:e230. doi:10.1371/journal.pbio.0060230.
70. **Goswami S, Sahana N, Pandey V, Doblas P, Jain RK, Palukaitis P, Canto T, Praveen S.** 2012. Interference in plant defense and development by nonstructural protein NSs of *Groundnut bud necrosis virus*. Virus Res. **163**:368–373.